AD-A138 015 MEASUREMENT OF HYDROACOUSTIC PARTICLE MOTION BY HOT-FILM ANEMOMETRY(U) NAVAL RESEARCH LAB WASHINGTON DC P S DUBBLEDAY 10 FEB 84 NRL-MR-5223 1/1

UNCLASSIFIED F/G 20/7 NL

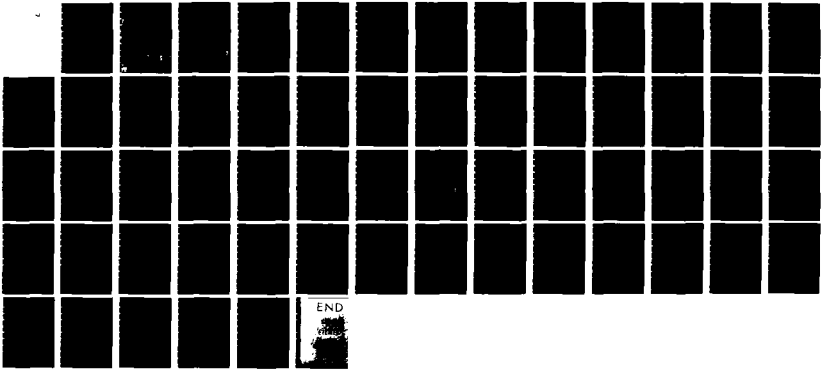

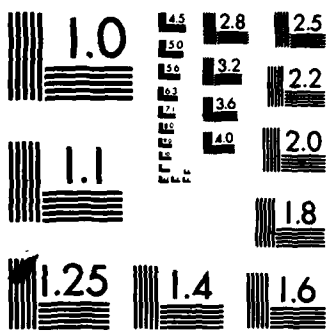

NRL Memorandum Report 5223

Measurement of Hydroacoustic Particle Motion by Hot-Film Anemometry

Pieter S. Dubbleday

Underwater Sound Reference Detachment
P.O. Box 8337
Orlando, Florida 32856

February 10, 1984

NAVAL RESEARCH LABORATORY
Washington, D.C.

Unclassified

SECURITY CLASSIFICATION OF THIS PAGE (When Data Entered)

REPORT DOCUMENTATION PAGE	READ INSTRUCTIONS BEFORE COMPLETING FORM
1. REPORT NUMBER: NRL MEMORANDUM REPORT 5223	2. GOVT ACCESSION NO. A138 015
	3. RECIPIENT'S CATALOG NUMBER
4. TITLE (and Subtitle): MEASUREMENT OF HYDROACOUSTIC PARTICLE MOTION BY HOT-FILM ANEMOMETRY	5. TYPE OF REPORT & PERIOD COVERED: Interim report on continuing project
	6. PERFORMING ORG. REPORT NUMBER
7. AUTHOR(s): Pieter S. Dubbelday	8. CONTRACT OR GRANT NUMBER(s)
9. PERFORMING ORGANIZATION NAME AND ADDRESS: Underwater Sound Reference Detachment, Naval Research Laboratory, P.O. Box 8337, Orlando, FL 32856	10. PROGRAM ELEMENT, PROJECT, TASK AREA & WORK UNIT NUMBERS: PE 61153N, RR011-08-42, WU 0589-00
11. CONTROLLING OFFICE NAME AND ADDRESS: Office of Naval Research NNSFP Funds to Condensed Matter & Radiation Science Div. of Naval Research Laboratory, Washington, DC 20375	12. REPORT DATE: 10 February 1984
	13. NUMBER OF PAGES: 58
14. MONITORING AGENCY NAME & ADDRESS (if different from Controlling Office)	15. SECURITY CLASS. (of this report): Unclassified
	15a. DECLASSIFICATION/DOWNGRADING SCHEDULE

16. DISTRIBUTION STATEMENT (of this Report)
Approved for public release; distribution unlimited.

17. DISTRIBUTION STATEMENT (of the abstract entered in Block 20, if different from Report)

18. SUPPLEMENTARY NOTES

19. KEY WORDS (Continue on reverse side if necessary and identify by block number)
Acoustic particle motion
Hot-film anemometry
Heat transfer in acoustic field
Free convection about cylinder

20. ABSTRACT (Continue on reverse side if necessary and identify by block number)
The parameter most often measured in acoustic fields is the pressure. Other scalar field variables, like the density or temperature, may be directly computed from the pressure fluctuations at one point. To determine the particle velocity vector, one needs to know the pressure in the neighborhood of a given point in order to derive the acceleration by numerically computing the gradient field of the pressure. One may measure the velocity field more directly by recording the effect of accelerators attached to a neutrally —
(over)

20. Abstract (cont'd.)
buoyant sphere that follows the particle motion more or less closely. Its sensitivity to velocity, therefore, will be inversely proportional to the frequency.

Hot-film (or hot-wire) anemometry is based on the phenomenon that the heat transfer from an electrically heated film or wire is a function of the fluid motion past the sensor. It is extensively used in study of turbulence, where it is assumed that there is an exponential relation between heat flux and particle velocity, indicated as King's law. In an acoustic field of moderate intensity a different regime prevails: free convection cannot be ignored, and the periodicity in harmonic excitation implies that the same fluid is repeatedly carried past the sensor, without cooling to ambient temperature.

The importance of free convection implies a different mode of operation of the anemometer in horizontal or in vertical acoustic particle motion. In the first case the received frequency is twice that of the acoustic field, and the voltage is proportional to the square of the particle displacement. In the second case the frequency is equal to that of the field, and the voltage is linear in the particle displacement. The sensitivity and directional response may be increased by an imposed bias flow.

This report describes the measurement of the anemometer output in horizontal and vertical particle motion for water and ethylene glycol. The results are represented in terms of the nondimensional heat flow as a function of relative particle displacement, Fourier number, and Grashof number. The sensitivity to velocity increases with decreasing frequency and, therefore, the method is quite useful at low frequencies.

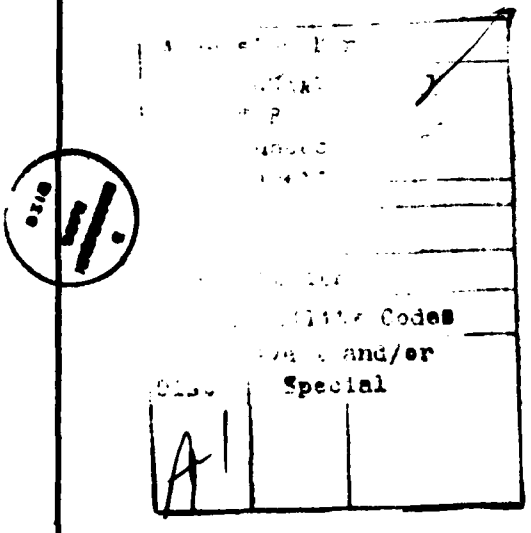

CONTENTS

LIST OF SYMBOLS

a	coefficient in linear relation for vertical motion, $Nu_{ac} = a(\zeta/d)$
b	coefficient in quadratic relation for horizontal motion, $Nu_{ac} = b(\xi d)^2$, b_m = measured value, b_c = calculated value
c	coefficient in experimental empirical relation
c_p	specific heat at constant pressure
d	diameter of hot-film sensor
g	acceleration of gravity
h	water depth in calibrator and trough
H	heat flux
$\vec{k}$	unit vector, vertically up
k	thermal conduction coefficient
ℓ	length of hot-film sensor
m	exponent in empirical relation
p	pressure
$\dot{Q}$	heat transfer rate
T	temperature (variable)
T_o	temperature of undisturbed medium (constant)
u,v,w	components of velocity vector $\vec{u}$
U	typical speed in imposed flow
U_{cr}	critical speed separating free and forced convection regimes
V_{ac}	rms value of ac voltage output from anemometer
α	$-\frac{1}{V}\left(\frac{\partial V}{\partial T}\right)_p$, thermal expansion coefficient, V is volume
Θ	$T - T_o$, temperature difference
Θ_s	temperature difference between sensor and undisturbed medium
κ	thermal diffusivity, $\kappa = \frac{k}{\rho c_p}$

LIST OF SYMBOLS (cont'd.)

ν	kinematic viscosity
ξ,η,ζ	components of displacement vector, $\vec{\xi}$
ρ	fluid density (variable)
ρ_o	fluid density at temperature T_o (constant)
ω	angular frequency of acoustic field

Dimensionless Numbers

Fo	Fourier number, $Fo = \frac{\kappa}{d^2\omega}$, compares heat conduction with local heating in periodic flow.
Gr	Grashof number, $Gr = \frac{g\alpha\Theta d^3}{\nu^2}$, compares advective acceleration with viscosity in free convection.
Nu	Nusselt number, $Nu = \frac{Hd}{k\Theta}$, nondimensional form of heat flux
Pe	Peclet number, $Pe = \frac{Ud}{\kappa}$, compares heat advection with conduction in forced convection.
Pr	Prandtl number, $Pr = \frac{\nu}{\kappa}$, compares diffusion of momentum with diffusion of heat
Ra	Rayleigh number, $Ra = \frac{g\alpha\Theta d^3}{\nu\kappa}$, compares buoyancy with viscosity and effect of heat conduction, $Ra = Gr\ Pr$.
Re	Reynolds number, $Re = \frac{Ud}{\nu}$, compares advective acceleration with viscosity.
Ri	Richardson number, $Ri = \frac{g\alpha\Theta d}{U^2}$, compares buoyancy with advective acceleration.
St	Stokes number, $St = \frac{\nu}{d^2\omega}$, compares viscosity with local acceleration in periodic flow.

MEASUREMENT OF HYDROACOUSTIC PARTICLE MOTION BY HOT-FILM ANEMOMETRY

INTRODUCTION

Most hydroacoustic detectors are sensitive to pressure fluctuations. When the acoustic field is simple and of known signature, one may compute particle velocity from a single local pressure measurement. For more complicated fields it is necessary to map the pressure field in both magnitude and phase in order to derive the particle acceleration by spatial differéntiation. It is attractive to measure the particle motion independently, as a check on the computations and as an alternate method of acoustic measurement. Examples of such measurements are given in References 1 and 2.

The method of hot-film or hot-wire anemometry offers a new approach to the detection of particle motion in acoustic fields in liquids and gases [3]. It determines the amount of heat transfer from an electrically heated film or wire to the surrounding fluid medium. This heat transfer depends on a number of factors, but under the proper conditions it is predominantly a function of the kinematic parameters of the fluid particles in the medium. Review articles on this technique are found in References 4, 5, and 6.

The method of hot-film anemometry has found application wherever its fast response time and small physical size are of advantage. Thus it has become the measurement device of choice in the study of turbulence. To the best of the author's knowledge, no other reports on application of hot-film anemometry to hydroacoustics are found in the literature. A computer search by the Defense Technical Information Center did not produce any relevant articles. There is extensive literature on the influence of intense acoustic fields or of the vibration of a given body on its heat transfer characteristics [7-12], but no mention is made of the principle of using the heat transfer to measure the acoustic radiation for its own sake.

It appears to be tacitly assumed in practically all applications of hot-film anemometry that the operation of the device may be described by the precepts of the forced convection regime. As a consequence the calibration relations are cast in the form of a relation between output voltage and imposed velocity, usually as a variation on King's law [13]. Two aspects of acoustic particle motion militate against application of the same type of relation in this case. First, the particle speeds are quite small for acoustic fields of modest intensity so that free convection is not negligible. Secondly, the periodicity implies that the same fluid will repeatedly pass by the sensor with only incomplete cooling by the ambient fluid during one period.

A theoretical analysis of the flow and heat transfer phenomena in the presence of an acoustic field appears quite formidable. In order to create a scheme for arranging calibration measurements, use is made of the dimensionless numbers that appear when a dimensional analysis is made of the equations of motion and heat diffusion.

The existence and importance of free convection lead to various modes of operation of hot-film anemometry in hydroacoustics. When the acoustic velocity is parallel to gravity, the free convection acts as a dc bias flow for the acoustic velocity. Therefore, the anemometer response is expected and found to have a frequency equal to the acoustic frequency and an amplitude proportional to the particle motion. When the acoustic velocity is horizontal, it is not accompanied by a dc bias flow. Because of the symmetry of the physical situation for the movement of the particles to one side or the other of the sensor, one expects an anemometer response with twice the frequency of the acoustic field and an amplitude proportional to the square of the particle motion.

A third mode of operation of the anemometer may be induced by creating an imposed dc bias flow by a nozzle that directs a jet of fluid onto the sensor. The sensitivity of the instrument is thereby increased, and one is largely free from the dependence on the direction of gravity. The direction of this jet determines a preferred direction which improves the directional properties of the anemometer. A second directional sensitivity is supplied by the axis of the cylindrical sensor: the preferred direction for the flow is perpendicular to this axis for all three modes of operation.

The next section offers a theoretical analysis and a formulation of the pertinent dimensionless numbers. The creation and calibration of flow fields needed to test the anemometer are described, and the data are given as a function of the relevant dimensional parameters. A comprehensive view of the data is given by empirical relations in terms of dimensionless numbers. The computation of the various dimensionless numbers is discussed in Appendix A. Appendix B describes the construction of a trough and shaker arrangement used to produce horizontal particle motion.

1. THEORETICAL ANALYSIS

1.1. Basic Equations and Processes

The fundamental equations that govern the phenomenon of heat transfer in hot-film anemometry are the conservation of mass, the equation of motion, and the conservation of energy. Usually these equations are presented in a simplified form, known as the Boussinesq approximation [14,15]. The continuity equation

$$\frac{\partial \rho}{\partial t} + \vec{\nabla} \cdot (\rho \vec{u}) = 0, \tag{1}$$

(where ρ is the density of the medium and $\vec{u}$ is the particle velocity vector) is simplified to the incompressibility relation

$$\vec{\nabla} \cdot \vec{u} = 0. \tag{2}$$

The suppression of the time derivative of the density even in the presence of acoustic radiation is based on the fact that the size of the sensor is small compared with the wavelength of sound in the region studied.

The equation of motion in this approximation is

$$\frac{\partial \vec{u}}{\partial t} + (\vec{u} \cdot \vec{\nabla})\, \vec{u} = -\frac{1}{\rho_o} \vec{\nabla} p + g\alpha\Theta\vec{k} + \nu\nabla^2\vec{u}, \tag{3}$$

where $\alpha = (1/V)(\partial V/\partial T)_p$ is the thermal expansion coefficient and V is volume;

$\Theta = T - T_o$, the difference between the local temperature and the temperature T_o of the undisturbed medium;

ν = kinematic viscosity;

ρ_o = density of the undisturbed medium (constant);

g = acceleration of gravity;

$\vec{k}$ = a unit vector vertically upward; and

p = dynamic pressure.

The conservation of energy reduces to a temperature equation

$$\frac{\partial T}{\partial t} + (\vec{u} \cdot \vec{\nabla})T = \kappa \nabla^2 T, \tag{4}$$

where κ is the thermal diffusivity equal to $k/\rho c_p$, with k the heat conduction coefficient and c_p the specific heat at constant temperature. The approximation implied by Eqs. (3) and (4) amounts to setting all physical parameters of the medium constant except the density insofar as it causes buoyancy. The density difference in the buoyancy term is approximated by a linear expression in the temperature or $\frac{\Delta\rho}{\rho_o} = -\alpha\theta$.

The measurement of acoustic particle motion by means of hot-film anemometry consists of two interacting processes. The heat transfer from the hot film in a quiescent fluid, in addition to the ever-present heat conduction, is due to convection by the buoyancy of the fluid that is heated by the film itself. This process is called free convection. The second process is that of an incompressible fluid motion about the cylindrical sensor accompanying the acoustic radiation.

The first process may be described by Eqs. (2), (3), and (4), where the time derivatives $\partial\vec{u}/\partial t$ and $\partial T/\partial t$ are omitted, since the fluid motion near the cylinder is steady and becomes unstable only several diameters away from the cylinder. The equation of motion, Eq. (3), and the temperature equation, Eq. (4), are coupled and have to be solved simultaneously. This cannot be done analytically, even for simple geometries; one has to rely on empirical relationships [16-18]. The second process, flow past a cylinder perpendicular to the flow, is more amenable to analytical or numerical treatment. Unfortunately, even with more-or-less extensive knowledge of the two separate processes it is, in general, not possible to add their effects because of the nonlinear advective acceleration $(\vec{u} \cdot \vec{\nabla})\vec{u}$. In case this term is small compared with local acceleration $\partial\vec{u}/\partial t$, one may add the two solutions for the

free convection and imposed acoustic flow. One might intuitively feel that the horizontal particle motion due to the acoustic field is reasonably independent of the motion due to the thermal plume in the free convection and could be independently solved, as if it were forced convection. The resulting velocity field could then be introduced into the temperature equation and solved for the relevant heat transfer.

1.2. Dimensional Analysis

The complexity of the equations governing the heat transfer by a hot film, in the presence of acoustic radiation, renders the analytical or numerical solution a formidable task. In order to establish a calibration of the hot-film anemometry to serve as a tool in acoustic research, one may utilize the concepts of dimensional analysis to reduce the number of variables influencing the phenomenon to a smaller set of dimensionless groups. For reference, Eqs. (3) and (4) are repeated here, with a short description of the meaning of each term written under the equation.

Equation of Motion:

$$\frac{\partial \vec{u}}{\partial t} + (\vec{u} \cdot \vec{\nabla})\vec{u} = -\frac{1}{\rho_o}\vec{\nabla}p + g\alpha\theta\vec{k} + \nu\nabla^2\vec{u} \qquad (5)$$

local acceleration	advective acceleration	pressure force	buoyancy	viscosity

Temperature Equation:

$$\frac{\partial T}{\partial t} + (\vec{u} \cdot \vec{\nabla})T = \kappa\nabla^2 T \qquad (6)$$

local heating rate	advection of heat	conduction of heat

Dimensional analysis consists in comparing the order of magnitude of the various terms. The ensuing dimensionless groups serve as the independent variables in the sought-for empirical relations.

The relevant dependent variable is the heat flux H, expressed in dimensionless form by the Nusselt number $Nu = (Hd/k\Theta_s)$, where d is the diameter of the sensor and $\Theta_s = T_s - T_o$ is the difference in temperature between sensor and undisturbed medium.

1.3. Forced Convection Versus Free Convection

An important distinction in heat transfer by fluids is that between forced convection and free convection. In the first case there is an imposed flow of sufficient strength to make the buoyancy term negligible. The equation of motion then is not coupled to the temperature equation and the equation of motion may be independently solved. The solution for the velocity field is entered into the temperature equation through the advected heat term $\vec{u} \cdot \vec{\nabla}T$, and this equation is then solved for the temperature. In free convection the two equations have to be solved simultaneously, since the term driving the motion is the buoyancy itself. For the present application the distinction is important since one likes to know what the value of an imposed bias flow may be in order to qualify for the designation of forced convection.

Suppose that a bias flow with typical speed U is imposed on the sensor. To judge its significance one compares the buoyancy term $g\alpha\Theta_s$ in Eq. (5) with either the advective acceleration term $(\vec{u} \cdot \vec{\nabla})\vec{u}$ or the viscosity term $\nu\nabla^2\vec{u}$, depending on which of these is dominant. The relevant dimensionless group to compare advective acceleration (inertia) with viscosity is the Reynolds number $Re = Ud/\nu$. If $Re \gg 1$, one compares buoyancy with inertia, which results in the Richardson number $Ri = g\alpha\Theta d/U^2$. If $Re \ll 1$, one compares buoyancy with viscosity and the pertinent number is $g\alpha\Theta d^2/U\nu$, equal to RiRe (no separate name was found for this dimensionless group). Thus forced convection is present if $Re \gg 1$ and $Ri \ll 1$, or if $Re \ll 1$ and $ReRi \ll 1$. Free convection prevails if $Re \gg 1$ and $Ri \gg 1$, or $Re \ll 1$ and $ReRi \gg 1$. Any intermediate case is called mixed convection. The borderline speed U_{cr} is obtained by setting either $Ri = 1$ and solving for U, or by setting $ReRi = 1$, depending on whether this given U_{cr} makes $Re > 1$ or $Re < 1$, respectively.

In Table 1 the values of U_{cr} are given for the three sensor diameters and three temperature differences between sensor and medium used in this study. Both water and ethylene glycol were studied. Except for the point marked with an asterisk, viscosity dominates over inertia. In Table 2 values for U are

given that make the Reynolds number equal to 1. The importance of this table is that one may judge for which values of U the convection is of the forced type, while still Re<1. The latter condition defines a flow regime known as creeping flow. For such flow about a cylinder, Stokes has given an analytic solution, refined by Oseen [19,20]. Thus, in some cases of an imposed flow with the proper speed, one may use this analytic solution, insert it into the temperature equation, and find a solution of the latter, presumably in numeric form. Usually, though, one has to settle for an empirical relation for the given heat transfer in terms of the relevant dimensionless number(s). For heat transfer from a cylinder, this is usually designated as "King's law", after the author of the first investigation into this subject [13].

Morgan [21] proposes a relation of the form

$$Nu = (C + D\ Re^{n})\ Pr^{p}, \tag{7}$$

where Pr is the Prandtl number $Pr = \nu/\kappa$, and lists values for the constants C, D, n, and p from many sources. Blackwelder [22] writes the relation in a more general form

$$Nu = [A(Pr,a_T) + B(Pr,a_T)Re^{n}]\ (1 + a_T/2)^{m}, \tag{8}$$

where a_T is the overheat ratio $a_T = \Theta_s/T_o$ (T_o in Kelvin).

The aspect ratio ℓ/d, where ℓ is the length of the sensor, would also be expected to be important. This is especially true for hot films, where this ratio is much smaller than for wires, and thus the conditions are farther removed from the ideal case of an infinite cylinder.

This proliferation of dimensionless numbers and relations was addressed by Blackwelder [22] in a thoughtful comment:

> "It is distressing (especially to the uninitiated) that there is such a lack of agreement concerning the basic equation of hot-wire anemometry... These variations and deviation from an exact universal equation necessitate that each hot-wire and hot-film be calibrated individually...before it can be used to record and interpret data."

This quote may warn against too optimistic a hope of finding a comprehensive empirical equation for all circumstances of sensor type, frequency, temperature, and medium in the application to hydroacoustics.

The Eqs. (7) and (8) may be used to relate particle speed to measured dc voltage in the case of imposed bias flow.

Table 1 - Critical speed U_{cr} in mm/s as a function of sensor diameter d and temperature difference Θ_s. For $U \gg U_{cr}$ forced convection obtains, for $U \ll U_{cr}$ free convection. The values for U_{cr} are found from ReRi = 1, except the point marked *, where Ri = 1.

Θ_s ↓	Water ---------> d in μm			Ethylene glycol		
°C	25	50	150	25	50	150
15	0.039	0.15	1.4	0.0051	0.021	0.19
30	0.11	0.43	3.9	0.014	0.057	0.51
45	0.21	0.85	5.4*	0.029	0.11	1.0

Table 2 - Speed U in mm/s for which Re = 1. For Re<1 one may apply the results of Stokes and Oseen for creeping flow [19,20]

Θ_s ↓	Water ---------> d in μm			Ethylene glycol		
°C	25	50	150	25	50	150
15	30.8	15.4	5.13	474	237	79
30	26.3	13.2	4.39	348	174	58
45	22.8	11.4	3.81	258	129	43

1.4. Free Convection

By definition the term free convection implies that the buoyancy term $g\alpha\Theta$ dominates the equation of motion. The Reynolds number still would be important to distinguish between inertia-dominated and viscosity-dominated flow regimes. Obviously Re cannot be directly evaluated since the value of U is not known a priori. It has, in turn, to be estimated from dimensional considerations. The buoyancy term must be matched by either advection or viscosity in the equation. If buoyancy and advection match, the value of U is $U \approx (g\alpha\Theta d)^{1/2}$ and inserting this U into the Reynolds number gives a group $[(g\alpha\Theta d^3)/\nu^2]^{1/2}$. If buoyancy and viscosity match, one has $U \approx (g\alpha\Theta d^2)/\nu$ and the Reynolds number is transformed into $(g\alpha\Theta d^3)/\nu^2$. The Grashof number is defined by $Gr = (g\alpha\Theta d^3)/\nu^2$ and one sees that it takes the place of the Reynolds number: inertia dominates for large Grashof number, viscosity dominates for small Gr, with the understanding that the situation is one of free convection where the buoyancy term is the prime mover.

One may apply the same reasoning to the Péclet number, which compares heat advection with heat conduction. It follows that the product GrPr takes the place of the Péclet number for small Gr; for large Gr it is the combination $Gr^{1/2}\,Pr$. The product GrPr is also known as the Rayleigh number, $Ra = GrPr = (g\alpha\Theta d^3)/\nu\kappa$.

An empirical relation connecting heat transfer to the independent variables in free convection is given by Morgan [23], who lists values for the constants A, B, m from various sources, as

$$Nu = A + B\,(GrPr)^m. \tag{9}$$

This relation is used to interpret dc heat transfer in Section 3.1. Jaluria [24] gives a relation $Nu = C(GrPr)^{1/4}$ where C is a function of the Prandtl number.

1.5. Response to Acoustic Fields

It was assumed in the foregoing sections that the phenomena were steady. The instabilities in the thermal flow were ignored, since they appear only several diameters away from the sensor. If one introduces a harmonic acoustic particle motion with angular frequency ω, the time derivatives in Eqs. (5) and

(6) are to be reckoned with. The first dimensional estimate concerns the ratio of advective acceleration to the local derivative, resulting in the dimensionless number $U/\omega d$, where U is the rms value of a harmonic vibration. If one introduces the rms displacement vector $\vec{\xi}$ with components ξ, η, ζ, this may also be written as ξ/d and ζ/d for horizontal and vertical acoustic motions, respectively.

For horizontal particle motion there is symmetry for the motion to the right or to the left of the film. Therefore, one expects that the frequency of the anemometer response is twice the frequency of the acoustic field. Moreover, the first term in an expansion of the response in powers of relative displacement would be quadratic. Thus, for modest values of the relative displacement, one expects that the Nusselt number varies harmonically with twice the frequency of the field, and that the rms value of the fluctuating component Nu_{ac} is given by

$$Nu_{ac} = b(\xi/d)^2, \tag{10}$$

where the coefficient b is independent of the displacement ξ. Nu_{ac} is proportional to the rms value of the ac voltage V_{ac}. For the vertical particle motion of the acoustic field there is a dc bias flow provided by the free convection. Therefore, one expects the frequency of the response to be the same in this case as that of the acoustic field and the Nusselt number variation to be linear in the displacement for modest values of this parameter. Thus,

$$Nu_{ac} = a(\zeta/d), \tag{11}$$

where the coefficient a is independent of the displacement ζ. The coefficients a and b might be functions of the dimensionless numbers defining the free convection field Gr and Pr. It is found experimentally that the coefficient a is independent of frequency within the range covered by the experiments; the coefficient b, though, is dependent on frequency. Inspection of the temperature equation indicates that the relevant dimensionless number is the Fourier number $Fo = \kappa/\omega d^2$. It compares the heat carried away by conduction with the local variation of stored heat in a fluid particle. Another frequency-dependent dimensionless number is the Stokes number $St = \nu/\omega d^2$,

which compares the viscosity with the local acceleration. Of course, one has St = FoPr. As in the case of steady flow, keep in mind the aspect ratio ℓ/d as another variable able to influence the anemometer response.

2. EXPERIMENTAL METHODS AND RESULTS

The experiments conducted with the hot-film anemometer fall into three categories. The response to horizontal particle motion is measured in a newly developed trough and shaker arrangement (see Appendix B). For vertical particle motion, the NRL-USRD type G40 calibrator is used [25]. The velocity field in the two devices is calibrated by an NRL-USRD type F61 standard hydrophone [25]. The pressure field is determined as a function of location; spatial differentiation then gives the acceleration according to the relation (Euler's equation)

$$\frac{\partial \vec{u}}{\partial t} = -\frac{1}{\rho_o} \vec{\nabla} p. \tag{12}$$

The third type of measurements consists of the response to acoustic motion, in the presence of a bias flow produced by a nozzle, in the G40 calibrator.

Figure 1 depicts the experimental arrangement. The hot-film anemometer is a ThermoSystems Inc. System No. 1050-1. The various sensors used in the experiment are shown in Fig. 2. The sensor type is designated by a number and letter combination; e.g., 1210-20W. Notice that the last two digits before the dash refer to the shape of the probe; the letter W indicates a quartz-coated film for use in conducting liquids. The two digits after the dash indicate diameter: 10 corresponds to 25 μ, 20 to 50 μ, and 60 to 150 μ. The oscillator is an HP3300A function generator with a 3305A sweep plug in. Its signal drives an Optimation Model PA250M power amplifier in constant current mode, which provides the power for driving the coil of the G40 calibrator or the shaker. A frequency reference signal is taken from a standard resistor in series with the coil and is entered into the reference input of the PAR Model 5204 Lock-In Analyzer. It is important that this reference signal not deviate too much from the optimum value of 1 V. The lock-in analyzer has a vector option to provide magnitude and phase of the anemometer output, the phase thus is relative to the phase of the current through the coil. The hot-film

anemometer output is viewed on an HP1200B oscilloscope, which shall be disconnected when measurements are taken with the F61 hydrophone in order not to shunt its high input impedance. The lock-in amplifier has a 1f - 2f setting so that the analyzed frequency may be taken as equal to the field frequency for vertical motion and twice the acoustic frequency for horizontal motion. The output signal from the lock-in, magnitude or phase, is plotted on an HP7015B X-Y recorder. The x coordinate is derived from the output of the sweep generator connected with the oscillator.

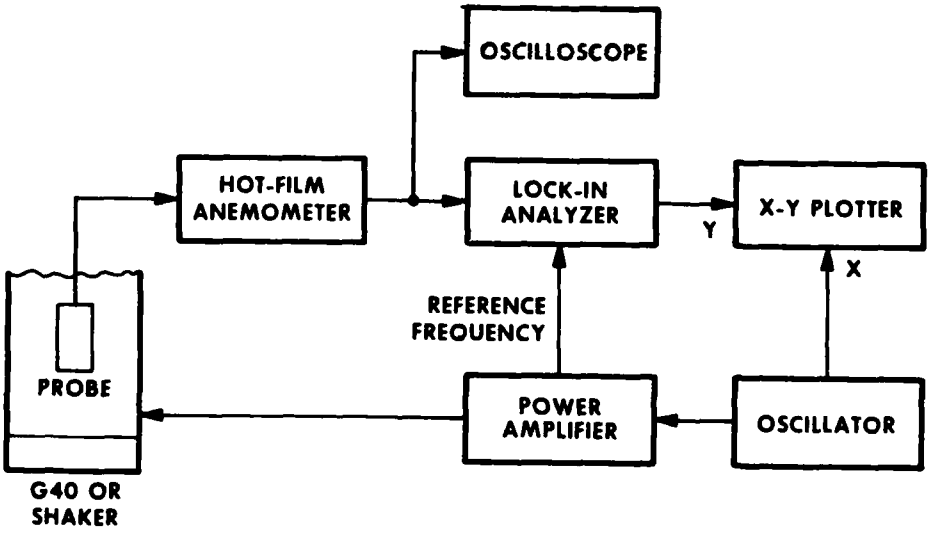

Fig. 1 - Block diagram for experimental arrangement

Configuration	Type	Size
Model 1210 Standard Straight Probe 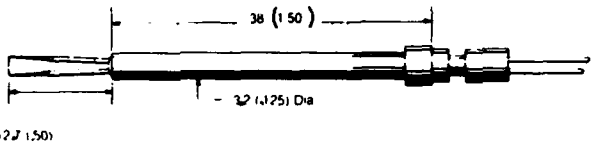	20 W	ℓ = 1 mm d = 50 μ
Model 1211 Sensor Parallel to Probe Cross Flow 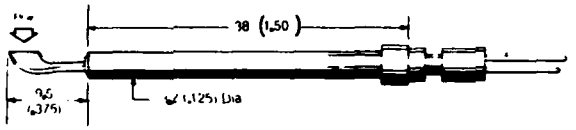	20 W	ℓ = 1 mm d = 50 μ
Model 1212 Probe with 90° Bend 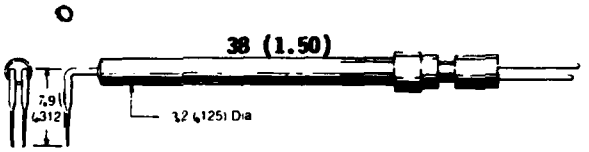	60 W	ℓ = 2 mm d =150 μ
Model 1260A Straight Probe-Miniature 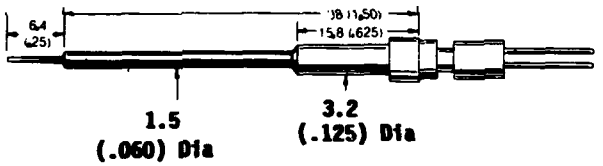	10 W	ℓ = 0.5 mm d = 25 μ

Legend: mm (in.)

Figure provided by courtesy of TSI Incorporated.

Fig. 2 - Sensors used in experiments

2.1. Horizontal Particle Motion

A trough and shaker arrangement was especially developed to create a horizontal periodic particle motion. It is described in Appendix B.

Although the measurements are performed in the center of the trough, where theoretically no vertical motion is present, a 1211 type sensor was used in the earlier measurements. This sensor is parallel to the probe and probe holder, and therefore is parallel to the direction of the free convection. It is expected that any spurious 1f signals would be attenuated this way, by virtue of the lesser sensitivity of the vertical sensor for vertical motion (see the discussion of vertical particle motion), by about a factor of four. It was found that no 2f signal is produced by whatever spurious signals are present. Thus the sensors with diameters of 25 and 150 μ were used in the configuration perpendicular to the vertical (z) direction (see Fig. B1).

A typical curve from the trough measurements is given in Fig. 3, both magnitude and phase. The frequency along the x axis is that of the acoustic field. The recorded frequency is twice this value. This should be kept in mind in observing e.g. electrically picked-up signals like those from the ac power lines. There is practically no phase shift between current through the coil and output from the pressure hydrophone. Thus the recorded phase from the anemometer is directly relative to the particle displacement. The pressure field is approximately independent of frequency in the given range. Thus the voltage output is roughly proportional to the inverse fourth power of the frequency. A comparison was made between the response of a 1211-20 sensor and a 1210-20 sensor. The difference is in the orientation. The 1211 sensor has its axis vertical (z direction); the 1210's is horizontal (y direction). There was no noticeable difference for the few cases where these were compared. This appears to indicate that there is no strong coupling between the heat transfer due to the horizontal motion and the vertical thermal plume (at least at the given $Gr = 6 \times 10^{-2}$): the convection is different for a vertical as compared with a horizontal cylinder (see Ref. 26). Shown in Table 3 is the sensitivity of the anemometer to rotation of the sensor in the plane of cylinder and particle motion direction. The x direction is the direction of horizontal particle motion; the z axis is vertical. One sees that there is a very strong, and therefore experimentally useful, directional effect at low frequency. It decreases drastically with increasing frequency, though.

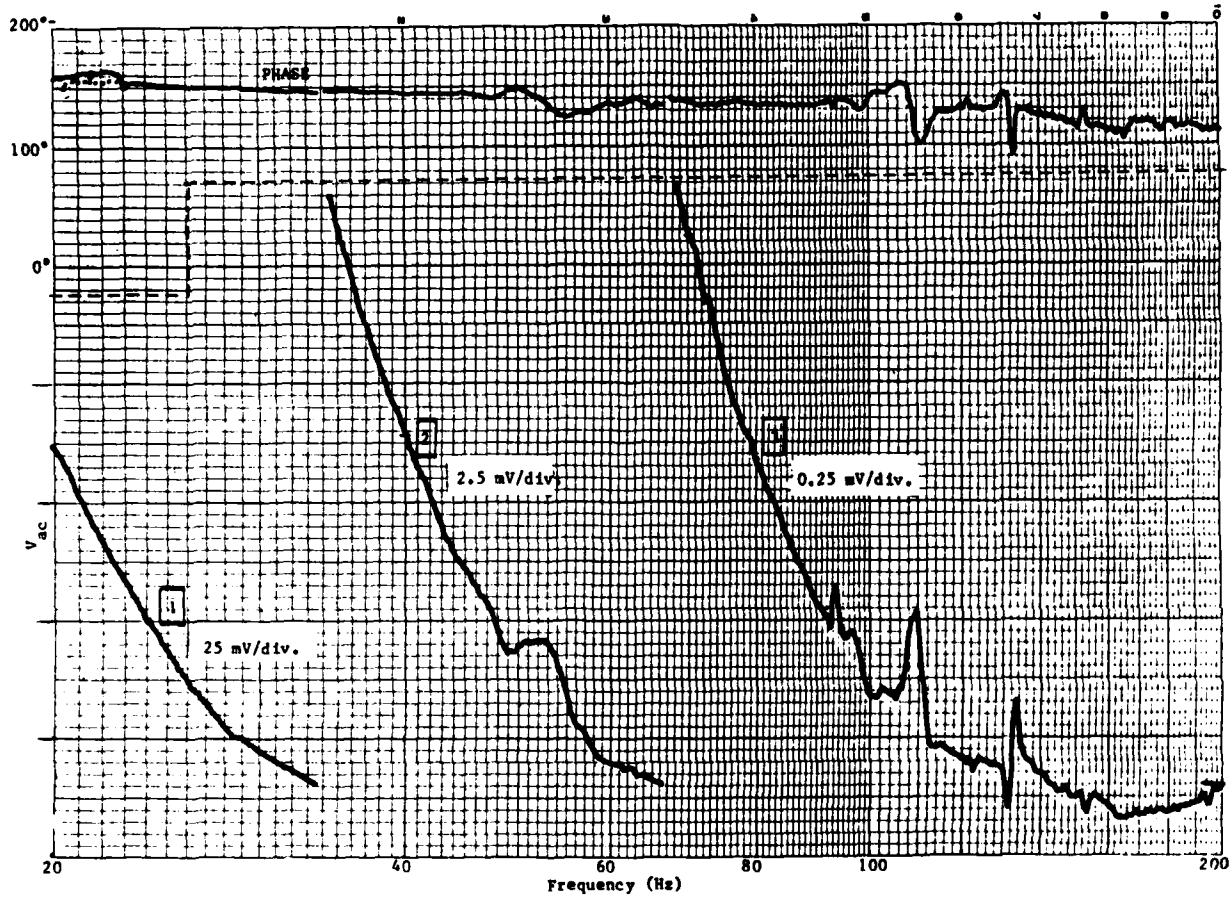

The frequency of the abscissa is that of the acoustic field. The received frequency is twice that amount. The upper curve shows phase and the curves 1, 2, 3 are magnitude at three settings of the analyzer:

1 - 25 mV/division
2 - 2.5 mV/division
3 - 0.25 mV/division

Sensor: 1211-20W; Θ_s = 30°C; 3A through coil.

Fig. 3 - Example of anemometer response in trough

Table 3 - Directional effect of anemometer response to horizontal motion in ethylene glycol. The direction of the motion is along the x axis; z is vertical. The values listed are V_{ac} in mV.

Sensor	Θ_s °C	Current Thru Coil	Direction	Frequency						
				20 Hz	40 Hz	60 Hz	80 Hz	100 Hz	120 Hz	140 Hz
1212-60	30	2A	45°	8.05	0.687	0.137	0.030	--	0.017	0.016
			x	1.15	0.087	0.032	0.020	0.015	0.012	0.012
			y	16.2	1.50	0.250	0.0875	0.0375	0.030	0.025
1260-10	30	2A	45°	9.87	0.912	0.225	0.077	0.023	0.015	0.010
			x	1.40	--	0.028	0.01	0.0062	0.0048	0.0040
			y	15.5	1.60	0.375	0.115	0.051	0.020	0.012
1210-20	30	2A	45°	22.0	1.75	0.370	0.122	0.040	0.033	0.019
			x	2.10	0.152	0.042	0.010	--	0.012	0.006
(1211-20)	30	2A	y	24.0	2.20	0.440	0.147	0.060	0.035	0.015

In Table 4 the velocities are given that refer to Tables 5 through 7. The speeds are in units of mm/s and are independent of the sensor used, since they are a function of the acoustic field only. They are approximately proportional to the inverse of the frequency.

Table 4 - RMS velocity u(mm/s), for water in trough as a function of frequency and current through shaker coil. (To be used with Tables 5-7.)

Frequency (Hz)	I = 1A	I = 2A	I = 3A
20	2.60	5.20	7.80
24	2.30	4.60	6.90
40	1.37	2.74	4.71
48	1.27	2.54	3.82
72	0.713	1.43	2.14
80	0.656	1.31	1.97
120	0.449	0.897	1.35
160	0.372	0.744	1.12

An overview of the data for water is given in Tables 5 through 7. The dependent variable is the relative displacement ξ/d computed from the pressure hydrophone calibration. The last two digits 10, 20, and 60 in the sensor designation indicate diameters of 25, 50, and 150 μm, respectively. Three temperature differences Θ_s between sensor and medium were chosen: 15, 30, and 45°C. The upper limit for usable temperature of the film is determined by the deleterious influence of air bubbles driven out of solution and adhering to the film and eventually boiling. The dependence of the output ac voltage on the relative displacement is expected to be quadratic, and b is the coefficient in the quadratic dependence of Nu_{ac} (proportional to V_{ac}) on the relative displacement. This is further discussed in Section 3.2 with the role of the Fourier number, which is an entry in the tables.

Table 5 - Hot-film anemometer output from horizontal particle motion in water; Θ_s = 15°C

			I = 1A		I = 2A		I = 3A			
	#	f Hz	ξ/d	V_{ac} mV	ξ/d	V_{ac} mV	ξ/d	V_{ac} mV	b 10^{-3}	Fo^{-1}
Sensor: 1260-10	1	20	0.827	5.45	1.65	20.0	2.48	37.0	6.00	0.531
V_{dc} = 2.40 V	2	24	0.616	3.00	1.22	11.0	1.83	22.0	6.17	0.638
Nu = 1.01	3	40	0.218	0.505	0.437	1.95	0.655	4.15	8.57	1.06
Pr = 5.44	4	48	0.169	0.275	0.337	1.10	0.506	2.35	8.07	1.28
Gr = 1.09×10^{-3}	5	72	0.0630	0.065	0.126	0.255	0.189	0.490	13.5	1.91
Nu_{ac}/V_{ac} = 0.845 V^{-1}	6	80	0.0522	0.050	0.104	0.170	0.157	0.335	13.4	2.13
	7	120	0.0238	0.014	0.0476	0.040	0.0714	0.072	15.9	3.19
	8	160	0.0148	0.008	0.0296	0.018	0.0444	0.030	21.2	4.25
Sensor: 1211-20	9	20	0.413	8.50	0.827	31.0	1.24	57.0	26.3	2.13
V_{dc} = 3.13 V	10	24	0.305	4.37	0.616	17.5	0.916	34.5	26.8	2.55
Nu = 0.934	11	40	0.109	0.812	0.218	3.25	0.328	6.00	38.3	4.25
Pr = 5.26	12	48	0.0843	0.400	0.169	1.60	0.253	3.35	32.8	5.10
Gr = 9.62×10^{-3}	13	72	0.0315	0.0987	0.0630	0.395	0.0945	0.800	58.4	7.65
Nu_{ac}/V_{ac} = 0.597 V^{-1}	14	80	0.0261	0.0762	0.0522	0.285	0.0783	0.535	60.4	8.50
	15	120	0.0119	0.0262	0.0238	0.068	0.0357	0.120	79.4	12.8
	16	160	0.00740	0.0162	0.0148	0.040	0.0222	0.060	119.0	17.0
Sensor: 1212-60	17	20	0.138	8.50	0.276	34.0	0.413	77.5	195	19.1
V_{dc} = 6.52 V	18	24	0.102	4.50	0.203	18.0	0.305	42.5	192	23.0
Nu = 1.41	19	40	0.0364	0.700	0.0728	2.80	0.109	6.50	232	38.3
Pr = 5.06	20	48	0.0281	0.360	0.0562	1.45	0.0843	3.45	203	45.9
Gr = 0.290	21	72	0.0105	0.075	0.0210	0.280	0.0315	0.70	292	68.9
Nu_{ac}/V_{ac} = 0.434 V^{-1}	22	80	0.00870	0.050	0.0174	0.190	0.0261	0.42	275	76.5
	23	120	0.00394	0.025	0.00793	0.047	0.0119	0.095	448	115
	24	160	0.00247	0.022	0.00493	0.030	0.00740	0.030	800	153

Table 6 - Hot-film anemometer output from horizontal particle motion in water; Θ_s = 30°C
Data in parentheses ignored; inconsistent.

			I = 1A		I = 2A		I = 3A			
		f		V_{ac}		V_{ac}			b	
	#	Hz	ξ/d	mV	ξ/d	mV	ξ/d	mV	10^{-3}	Fo^{-1}
Sensor: 1260-10	25	20	0.827	(16.2)	1.65	31.0	2.48	59.0	6.6	0.520
V_{dc} = 3.55 V	26	24	0.616	(8.62)	1.22	18.0	1.83	37.5	7.3	0.623
Nu = 1.12	27	40	0.218	(1.50)	0.437	3.25	0.655	6.50	10.1	1.04
Pr = 4.55	28	48	0.169	(0.837)	0.337	1.80	0.506	3.75	9.6	1.25
Gr = 3.61×10^{-3}	29	72	0.0630	(0.187)	0.126	0.425	0.189	0.850	15.9	1.27
Nu_{ac}/V_{ac} = 0.629 V^{-1}	30	80	0.0522	(0.130)	0.104	0.285	0.157	0.575	15.6	2.08
	31	120	0.0238	(0.0312)	0.0476	0.065	0.0714	0.140	17.7	3.12
	32	160	0.0148	(0.0125)	0.0296	0.025	0.0444	0.050	17.0	4.16
Sensor: 1211-20	33	20	0.413	10.7	0.827	43.0	1.24	87.5	28.1	2.08
V_{dc} = 4.84 V	34	24	0.305	5.62	0.616	25.5	0.916	50.0	29.0	2.49
Nu = 1.12	35	40	0.109	0.987	0.218	4.5	0.328	8.87	40.0	4.16
Pr = 4.44	36	48	0.0843	0.562	0.169	2.45	0.253	4.50	36.3	4.99
Gr = 3.07×10^{-2}	37	72	0.0315	0.137	0.0630	0.620	0.0945	1.20	66.0	7.48
Nu_{ac}/V_{ac} = 0.462 V^{-1}	38	80	0.0261	0.0950	0.0522	0.415	0.0783	0.837	66.0	8.31
	39	120	0.0119	0.0325	0.0238	0.095	0.0357	0.205	85.9	12.5
	40	160	0.00740	0.0212	0.0148	0.038	0.0222	0.105	119	16.6
Sensor: 1212-60	41	20	0.138	17.0	0.276	77.5	0.413	142.0	289	18.7
V_{dc} = 9.43 V	42	24	0.102	9.00	0.203	40.0	0.305	77.5	281	22.4
Nu = 1.49	43	40	0.0364	1.40	0.0728	6.40	0.109	12.4	347	37.4
Pr = 4.24	44	48	0.0281	0.750	0.0562	3.25	0.0843	6.50	304	44.9
Gr = 0.937	45	72	0.0105	0.155	0.0210	0.72	0.0315	1.45	473	62.3
Nu_{ac}/V_{ac} = 0.315 V^{-1}	46	80	0.00870	0.100	0.0174	0.45	0.0261	0.95	442	74.8
	47	120	0.00394	0.022	0.00793	0.12	0.0119	0.22	518	112.0
	48	160	0.00247	0.015	0.00493	0.055	0.00740	0.09	688	150.0

Table 7 - Hot-film anemometer output from horizontal particle motion in water: Θ_s = 45°C

			I = 1A		I = 2A		I = 3A			
	#	f Hz	ξ/d	V_{ac} mV	ξ/d	V_{ac} mV	ξ/d	V_{ac} mV	b 10^{-3}	Fo^{-1}
Sensor: 1260-10	49	20	0.827	11.6	1.65	35.0	2.48	85.0	7.9	0.508
V_{dc} = 4.56 V	50	24	0.616	6.6	1.22	20.5	1.83	53.7	8.6	0.610
Nu = 1.24	51	40	0.218	1.19	0.437	3.65	0.655	10.9	12.5	1.02
Pr = 3.84	52	48	0.169	0.662	0.337	2.05	0.506	6.12	11.8	1.22
Gr = 8.40×10^{-3}	53	72	0.0630	0.150	0.126	0.475	0.189	1.37	19.2	1.83
Nu_{ac}/V_{ac} = 0.542 V^{-1}	54	80	0.0522	0.105	0.104	0.320	0.157	0.937	19.2	2.03
	55	120	0.0238	0.0262	0.0476	0.075	0.0714	0.225	22.3	3.05
	56	160	0.0148	0.0097	0.0296	0.028	0.0444	0.087	21.8	4.07
Sensor: 1211-20	57	20	0.413	20.0	0.827	70.0	1.24	142.0	38.7	2.03
V_{dc} = 5.82 V	58	24	0.305	12.0	0.616	38.7	0.916	83.7	41.2	2.44
Nu = 1.08	59	40	0.109	1.95	0.218	7.62	0.328	17.5	60.3	4.07
Pr = 3.73	60	48	0.0843	0.95	0.169	3.75	0.253	8.50	49.4	4.88
Gr = 7.24×10^{-2}	61	72	0.0315	0.185	0.0630	1.00	0.0945	2.25	85.7	7.32
Nu_{ac}/V_{ac} = 0.372 V^{-1}	62	80	0.0261	0.115	0.0522	0.650	0.0783	1.55	81.9	8.14
	63	120	0.0119	0.045	0.0238	0.162	0.0375	0.387	113	12.2
	64	160	0.00740	0.028	0.0148	0.075	0.0222	0.212	159	16.3
Sensor: 1212-60	65	20	0.138	28.0	0.276	105	0.413	--	390	18.3
V_{dc} = 12.1 V	66	24	0.102	14.5	0.203	58.7	0.305	--	385	22.0
Nu = 1.65	67	40	0.0364	2.35	0.0728	7.50	0.109	18.0	462	36.6
Pr = 3.84	68	48	0.0281	1.20	0.0562	4.70	0.0843	9.0	389	43.9
Gr = 1.81	69	72	0.0105	0.265	0.0210	1.20	0.0315	2.12	661	65.9
Nu_{ac}/V_{ac} = 0.273 V^{-1}	70	80	0.00807	0.190	0.0174	0.78	0.0261	1.45	656	73.2
	71	120	0.00394	0.040	0.00793	0.17	0.0119	0.32	693	110
	72	160	0.00247	0.020	0.00493	0.080	0.0074	0.142	855	146

The variation of the coefficient b with frequency and sensor prompted the question what the influence of the viscosity and diffusivity might be. Therefore the experiments were repeated with ethylene glycol as the medium. It has a thermal diffusivity and expansion coefficient comparable to those of water, but the viscosity is an order of magnitude larger. The ratio of the kinematic viscosity coefficients at 40°C is 13; the ratio of the Prandtl numbers at 40°C is 21. These results are shown in Tables 9 through 11 while Table 8 gives the corresponding speeds.

Table 8 - RMS velocity (mm/s) for ethylene glycol in trough as a dimension of frequency and current through shaker coil. To be used with Tables 9-11.

f Hz	I = 1A	I = 2A	I = 3A
20	2.58	5.18	7.70
40	1.47	2.93	4.40
70	0.776	1.55	2.32
100	0.578	1.14	1.73
140	0.453	0.906	1.36

Table 9 - Hot-film anemometer output from horizontal particle motion in ethylene glycol; Θ_s = 15°C

			I = 1A		I = 2A		I = 3A			
	#	f Hz	ξ/d	V_{ac} mV	ξ/d	V_{ac} mV	ξ/d	V_{ac} mV	b 10^{-3}	Fo^{-1}
Sensor: 1260-10	73	20	0.820	1.92	1.64	7.19	2.45	15.0	3.64	0.838
V_{dc} = 1.60 V	74	40	0.234	0.175	0.467	0.725	0.701	1.65	4.58	1.68
Nu = 1.09	75	70	0.0706	0.022	0.141	0.0875	0.211	0.210	6.14	2.93
Pr = 134	76	100	0.0368	--	0.0726	0.025	0.110	0.049	5.97	4.19
Gr = 9.92×10^{-6}	77	140	0.0206	0.007	0.0412	0.0075	0.0618	0.012	10.9	5.87
Nu_{ac}/V_{ac} = 1.36 V^{-1}										
Sensor: 1211-20	78	20	0.410	2.50	0.820	9.50	1.23	20.0	12.7	3.35
V_{dc} = 1.95 V	79	40	0.117	0.195	0.234	0.825	0.351	1.80	13.2	6.71
Nu = 0.879	80	70	0.0353	0.035	0.0706	0.087	0.106	0.185	15.0	11.7
Pr = 131	81	100	0.0184	0.017	0.0368	0.025	0.0552	0.040	25.3	16.8
Gr = 8.39×10^{-5}	82	140	0.0103	0.015	0.0206	0.015	0.0309	0.015	47.7	23.5
Nu_{ac}/V_{ac} = 0.902 V^{-1}										
Sensor: 1212-60	83	20	0.137	1.40	0.273	5.60	0.410	13.2	48.8	30.2
V_{dc} = 3.95 V	84	40	0.0389	0.125	0.0779	0.40	0.117	1.75	58.9	60.4
Nu = 1.26	85	70	0.0117	0.037	0.0235	0.053	0.0353	0.150	100	106
Pr = 135	86	100	0.00613	0.037	0.0123	0.020	0.0184	0.112	308	151
Gr = 2.12×10^{-3}	87	140	0.00343	0.018	0.00687	0.025	0.0103	0.087	612	211
Nu_{ac}/V_{ac} = 0.639 V^{-1}										

Table 10 - Hot-film anemometer output from horizontal particle motion in ethylene glycol; Θ_s = 30°C

			I = 1A		I = 2A		I = 3A			
	#	f Hz	ξ/d	V_{ac} mV	ξ/d	V_{ac} mV	ξ/d	V_{ac} mV	b 10^{-3}	Fo^{-1}
Sensor: 1260-10	88	20	0.820	4.30	1.64	15.5	2.45	31.5	6.30	0.838
V_{dc} = 2.28 V	89	40	0.234	0.385	0.467	1.60	0.701	3.65	7.17	1.68
Nu = 1.12	90	70	0.0706	0.051	0.141	0.220	0.211	0.455	10.4	2.93
Pr = 98.9	91	100	0.0368	0.018	0.0726	0.051	0.110	0.127	10.9	4.19
Gr = 3.63×10^{-5}	92	140	0.0206	0.0035	0.0412	0.012	0.0618	0.029	7.48	5.87
Nu_{ac}/V_{ac} = 0.987 V^{-1}										
Sensor: 1211-20	93	20	0.410	5.20	0.820	24.0	1.23	41.5	20.8	3.35
V_{dc} = 2.84 V	94	40	0.117	0.420	0.234	2.20	0.351	4.00	20.4	6.71
Nu = 0.942	95	70	0.0353	0.045	0.0706	0.26	0.106	0.50	27.7	11.7
Pr = 99.3	96	100	0.0184	0.014	0.0368	0.06	0.0552	0.11	28.1	16.9
Gr = 2.88×10^{-4}	97	140	0.0103	0.005	0.0206	0.015	0.0309	0.035	28.5	23.6
Nu_{ac}/V_{ac} = 0.663 V^{-1}										
Sensor: 1212-60	98	20	0.137	--	0.273	16.2	0.410	--	101	30.2
V_{dc} = 5.69	99	40	0.0389	--	0.0779	1.50	0.117	--	115	60.4
Nu = 1.33	100	70	0.0117	--	0.0235	0.162	0.0353	--	137	106
Pr = 95.3	101	100	0.00613	--	0.0123	0.037	0.0184	--	116	152
Gr_f = 8.41×10^{-3}	102	140	0.00343	--	0.00687	0.025	0.0103	--	252	211
Nu_{ac}/V_{ac} = 0.466 V^{-1}										

Table 11 - Hot-film anemometer output from horizontal particle motion in ethylene glycol; Θ_s = 45°C

			I = 1A		I = 2A		I = 3A			
	#	f Hz	ξ/d	V_{ac} mV	ξ/d	V_{ac} mV	ξ/d	V_{ac} mV	b 10^{-3}	Fo^{-1}
Sensor: 1260-10	103	20	0.820	6.72	1.64	23.5	2.45	47.0	7.20	0.838
V_{dc} = 2.81	104	40	0.234	0.637	0.467	2.52	0.701	5.60	9.50	1.68
Nu = 1.16	105	70	0.0706	0.075	0.141	0.340	0.211	0.720	13.3	2.93
Pr = 73.2	106	100	0.0368	0.017	0.0726	0.082	0.110	0.190	11.9	4.19
Gr = 9.61×10^{-5}	107	140	0.0206	0.0062	0.0412	0.022	0.0618	0.049	11.1	5.87
Nu_{ac}/V_{ac} = 0.824 V^{-1}										
Sensor: 1211-20	108	20	0.410	9.25	0.820	35.0	1.23	65.0	27.7	3.35
V_{dc} = 3.52	109	40	0.117	0.80	0.234	3.30	0.351	6.62	31.6	6.71
Nu = 0.976	110	70	0.0353	0.097	0.0706	0.40	0.106	0.825	43.1	11.7
Pr = 71.8	111	100	0.0184	0.025	0.0368	0.10	0.0552	0.20	39.4	16.8
Gr = 7.96×10^{-4}	112	140	0.0103	0.012	0.0206	0.025	0.0309	0.050	39.4	23.5
Nu_{ac}/V_{ac} = 0.555 V^{-1}										
Sensor: 121-60	113	20	0.137	6.12	0.273	28.0	0.410	59.5	141.0	30.2
V_{dc} = 7.22	114	40	0.0389	0.60	0.0779	2.30	0.117	5.12	153.0	60.4
Nu = 1.45	115	70	0.0117	0.050	0.0235	0.27	0.0353	0.52	171.0	106.0
Pr = 70.7	116	100	0.00613	--	0.0123	0.070	0.0184	0.15	185.0	151.0
Gr = 2.21×10^{-2}	117	140	0.00343	0.017	0.00687	0.030	0.0103	0.037	328.0	211.0
Nu_{ac}/V_{ac} = 0.401 V^{-1}										

2.2. Vertical Particle Motion

The vertical particle motion is created in an NRL-USRD type G40 calibrator. The response of the anemometer is measured at the same frequency as that of the acoustic field. A typical curve is shown in Fig. 4. Thanks to the greater sensitivity of the anemometer in this configuration it was possible to obtain useful results up to 300 Hz. Since the pressure in the calibrator is practically independent of frequency, the response is roughly inversely proportional to the square of the frequency. The difference of the anemometer output phase and the phase of the pressure measurement is practically independent of frequency, with a value of 20°. The effect of direction on sensitivity was measured by comparing the response of a 1210 sensor with that of a 1211 sensor. The former is perpendicular to the particle motion, the latter is parallel. The ratio is about 4 at 100, 200, and 300 Hz.

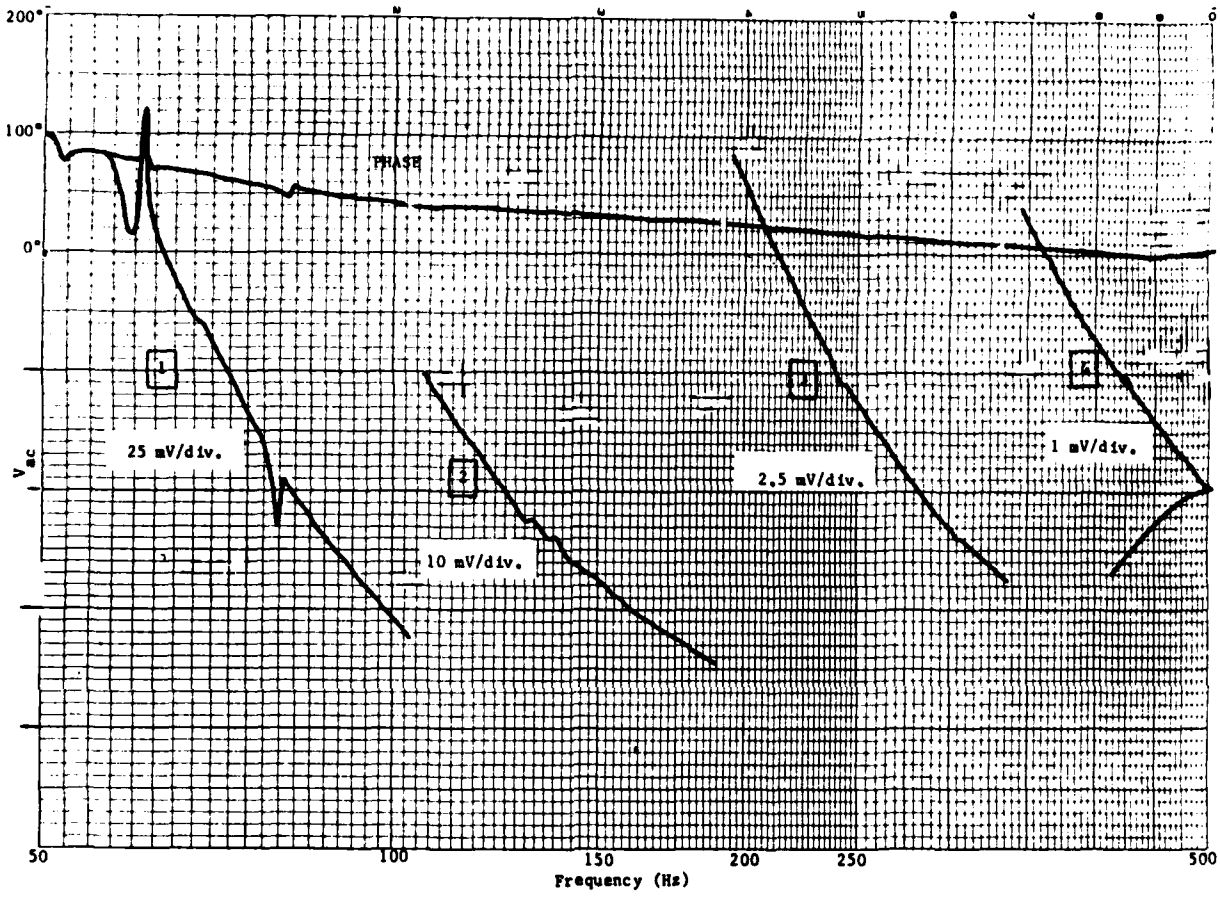

The frequency along the abscissa and that of the anemometer signal are the same, equal to the frequency of the acoustic field. The upper curve shows the phase, the curves 1, 2, 3, 4 magnitude.

1 - 25 mV per division
2 - 10 mV per division
3 - 2.5 mV per division
4 - 1 mV per division

Current through coil is 400 mA. Sensor 1210-20W, Θ_s = 45°C.

Fig. 4. Example of anemometer response in G40 calibrator.

The measurements were taken for water only. The results are shown in Tables 13 and 14. The two sets of data were taken about a year apart. Table 12 gives the velocities in mm/s corresponding to the displacements in Table 13. The dependence of the ac output voltage on relative displacement and other parameters is discussed in Section 3.3.

Some unusual problems were encountered during the experiments in the G40 calibrator. Bubbles were formed on the sensor, resulting in irreproducible and erratic behavior. This same type of problem had been encountered before. The experiments in the trough had not shown any of this trouble. It was realized that the only difference correlated with this behavior was the fact that the last series of G40 experiments, like the old set, was done after the water in the calibrator had been exposed to wiping off the walls with Aerosol OT100 surfactant (American Cyanamid Corp.). The proper operation of the anemometer was restored only after cleaning the calibrator, filling with fresh water, spraying the sensors with methylalcohol, and brushing with a fine paint brush. A full explanation was not attempted, but there is a strong suggestion that the surfactant, while aiding the release of a bubble that has been formed, promotes the formation of small bubbles on the hot sensor. The hot film in an air-saturated water medium creates a supersaturated air solution by increasing the local temperature. Bubbles may not be formed due to an energy barrier formed by the minimum bubble size that is energetically possible in connection with the very small radius of the sensor. If the surfactant reduces the specific surface energy, that energy barrier may be lowered. Even with these precautions the sensors were not totally reduced to their old status. Figure 5 shows another peculiar effect connected with this. Before brushing the sensor, the curve shows a very regular pattern of resonances above about 100 Hz. This certainly cannot be simple mechanical resonance of bubbles in the 1/2-mm size and smaller. But conceivably it is an effect of one or a whole series of bubbles that are compressed and expanded by the film at the acoustic frequency, the heat transfer changing periodically. Since heating of an insulator is a slow process, this might produce a low-frequency resonance. Further investigation of this effect would be of interest.

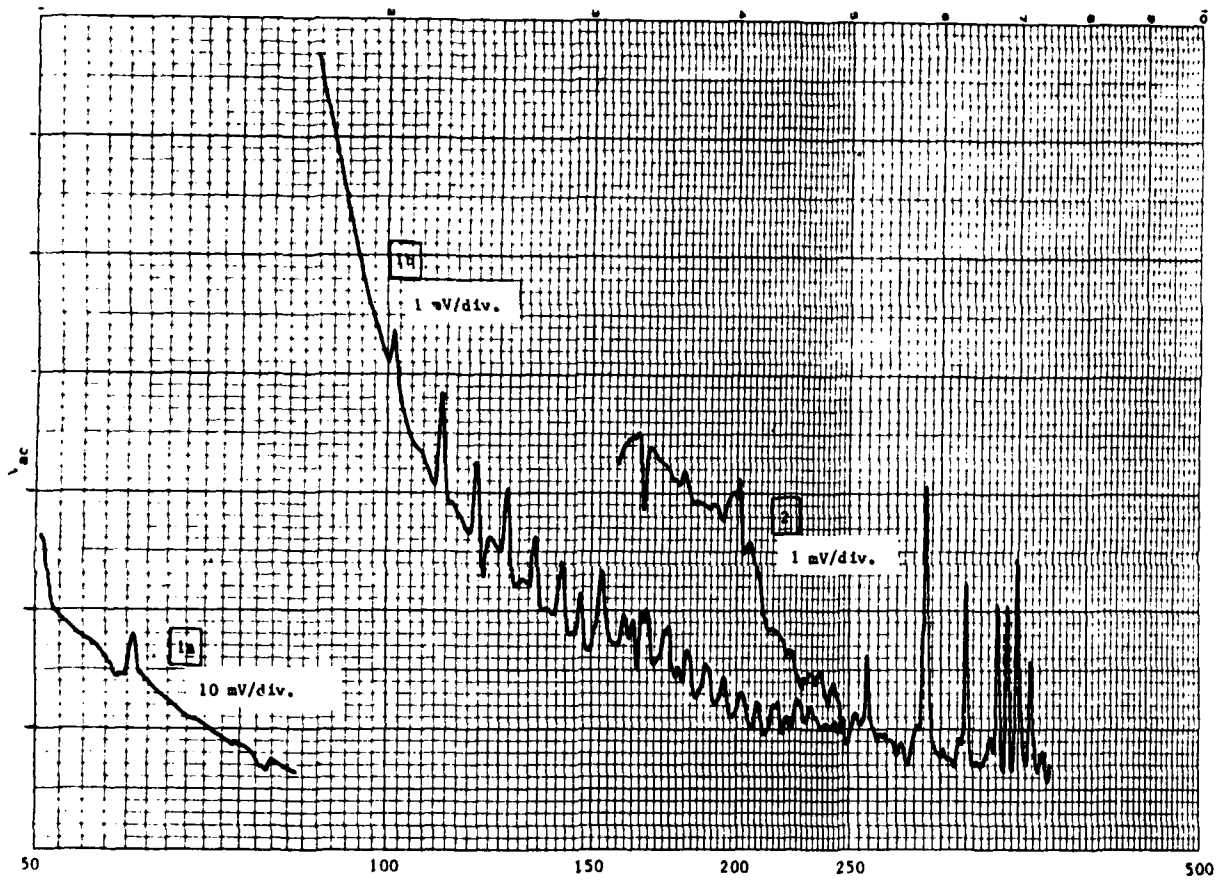

1 - before brushing: a - 10 mV/div
b - 1 mV/div

2 - after brushing

Sensor: 1210-20; Θ_s = 45°C; current through coil 0.1 A.

Fig. 5 - Effect of bubbles on sensor

Table 12 - RMS velocity (mm/s) for water in vertical calibrator as a function of frequency and current through calibrator coil. To be used with Table 13 (1982 data).

f Hz	I = .05A	I = .1A	I = .2A	I = .3A	I = .4A	I = .5A	I = .75A	I = 1A
20	0.99	1.98	3.96	5.94	7.92	9.90	14.8	19.8
40	1.45	2.90	5.81	8.71	11.6	14.5	21.8	29.0
60	1.10	2.21	4.41	6.62	8.82	11.0	16.5	22.0
80	0.88	1.75	3.50	5.26	7.01	8.76	13.1	17.5
100	0.705	1.41	2.82	4.23	5.64	7.05	10.6	14.1
120	0.567	1.13	2.27	3.40	4.54	5.67	8.51	11.3
140	0.510	1.02	2.04	3.06	4.08	5.10	7.65	10.2
160	0.362	0.725	1.45	2.17	2.90	3.62	5.44	7.25

Table 13 - Hot-film anemometer output from vertical particle motion in water.
Data of Jul & Aug 1982.

	f		V_{ac}		V_{ac}		V_{ac}		V_{ac}		V_{ac}	a
	Hz	ζ/d	mV	ζ/d	mV	ζ/d	mV	ζ/d	mV	ζ/d	mV	10^{-3}
		I = .05A		I = .1A		I = .2A		I = .4A				
Sensor: 1212-60	20	0.0524	37	0.105	65	--	--	--	--			219
Θ_s = 20°C	40	0.0385	32	0.0769	59	--	--	--	--			264
V_{dc} = 6.60 V	60	0.0195	17	0.0391	34	--	--	--	--			288
Nu = 1.09	80	0.0116	9	0.0233	18	0.0464	42	0.0930	72			267
Pr = 4.88	100	0.0075	6.2	0.0150	11.6	0.0299	26	0.0599	45			266
Gr = 0.428	120	0.0050	4.2	0.0100	8.4	0.0201	18	0.0401	26			267
Nu_{ac}/V_{ac} = 0.33 V^{-1}	140	0.0038	3.2	0.0077	6.5	0.0154	13	0.0308	21			265
	160	0.0030	2.5	0.0062	5.2	0.0123	10	0.0245	17			264
										#8 Average		263
		I = .1A		I = .3A		I = .5A		I = .75A		I = 1A		
Sensor: 1210-20	20	0.315	44	0.944	102	--	--	--	--	--	--	66.7
Θ_s = 30°C	40	0.231	30	0.692	75	1.15	65	--	--	--	--	63.0
V_{dc} = 4.67 V	60	0.117	17	0.351	47.5	--	--	--	--	--	--	74.1
Nu = 0.957	80	0.0697	10.2	0.209	29	0.349	47.5	0.523	92.5	0.697	132	83.4
Pr = 4.39	100	0.0449	6.8	0.135	19.5	--	--	0.337	47.5	0.449	82.5	82.1
Gr = 3.17×10^{-2}	120	--	--	--	--	0.150	23	0.225	18.7	0.301	45.0	68.0
Nu_{ac}/V_{ac} = 0.410 V^{-1}	140	0.0232	3.8	0.0674	10.5	--	--		--	0.232	32.5	84.2
	160	--	--	--	--	0.0721	11.5	--	--	--	--	66.3
										#9 Average		73.4
		I = .05A		I = .1A		I = .2A		I = .4A				
Sensor: 1212-60	20	0.0524	47	0.105	95	--	--	--	--			274
Θ_s = 30°C	40	0.0385	41	0.0769	70	--	--	--	--			301
Nu = 1.39	60	0.0195	23	0.0391	54	0.0780	110	--	--			403
Pr = 4.39	80	0.0116	12.5	0.0233	30	0.0464	55	0.0930	120.0			369
Gr = 0.856	100	0.0075	8.2	0.0150	20	0.0299	36	0.0599	75.0			372
Nu_{ac}/V_{ac} = 0.305 V^{-1}	120	0.0050	5.7	0.0100	14.2	0.0201	25	0.0401	47.0			381
	140	0.0037	4.6	0.0077	10.7	0.0154	21	0.0308	39.0			400
	160	0.0030	3.7	0.0062	10.5	0.0123	16	0.0245	31.0			419
										#10 Average		364

Table 14 - Hot-film anemometer output from vertical particle motion in water. Data of Jul 1983

Θ_s °C	Sensor	V_{dc} V	Nu	Pr	Gr	Nu_{ac}/V_{ac} V^{-1}	f Hz	I = .2A ζ/d	I = .2A V_{ac} mV	I = .4A ζ/d	I = .4A V_{ac} mV	a 10^{-3}	a (aver.) 10^{-3}
15°	1210-20	3.31	0.985	5.44	8.7×10^{-3}	0.595	100	0.0685	7.38	0.137	15.2	65.1	#1
							200	0.0181	2.08	0.0362	4.22	60.7	69.3
							300	0.0085	1.04	0.0170	2.14	73.9	
	1212-60	6.16	1.26	5.38	0.244	0.411	100	0.0228	7.05	0.0457	14.2	128.0	#2
							200	0.0060	2.00	0.0121	3.60	130.0	134
							300	0.0028	1.04	0.0057	1.90	145.0	
30°	1260-10	3.52	1.10	4.44	3.8×10^{-3}	0.626	100	0.137	6.05	0.274	15.2	31.3	#3
							200	0.0362	2.10	0.0724	4.95	39.6	35.4
							300	0.0170	(1.61)	0.0339	(4.15)	--	
	1210-20	4.96	1.11	4.55	2.88×10^{-2}	0.447	100	0.0685	15.5	0.137	32.0	103	#4
							200	0.0181	4.4	0.0362	9.13	111	108
							300	0.0085	2.0	0.0170	4.38	110	
	1210-60	8.92	1.33	4.49	0.804	0.299	100	0.0228	15.8	0.0457	29.0	198	#5
							200	0.0060	4.5	0.0121	8.13	213	209
							300	0.0028	2.1	0.0057	3.95	216	
45°	1210-20	6.15	1.14	3.84	6.72×10^{-2}	0.371	100	0.0685	22.8	0.137	48.0	127	#6
							200	0.0181	7.0	0.0362	14.0	144	140
							300	0.0085	3.5	0.0170	6.5	146	
	1212-60	10.9	1.33	3.80	1.86	0.245	100	0.0228	19.0	0.0457	40.1	210	#7
							200	0.0060	5.95	0.0121	10.7	230	234
							300	0.0028	2.95	0.0057	6.12	261	

(w is vertical velocity)

f Hz	I = .2A w(mm/s)	I = .4A w(mm/s)
100	2.15	4.30
200	1.13	2.27
300	0.80	1.60

The data taken in the G40 calibrator when presented as a function of the Grashof number fall on two different lines (see Sec. 3.3). This might be connected with the same bubble problem. No surfactant was used in the trough, and no bubble trouble was encountered there.

2.3. Imposed Bias Flow

A dc bias flow was imposed by means of a nozzle arrangement attached to a yoke. This way the direction of the water jet produced by the nozzle could be swung in a vertical plane, perpendicular to the hot film. The speed of the water jet was regulated by a needle valve. The water supply to the nozzle was gravity driven to ensure steady laminar flow. The experiments were done in the G40 calibrator where the particle motion is vertical. The value of the bridge voltage of the anemometer is a direct indication of the speed of the water jet. This was calibrated in a rotating tank. The relation between dc voltage and velocity may be described by an expression of the type given in Eq. (7) or (8). The diameter of the nozzle opening was 3 mm, and its front face was located 2 mm from the hot film. The results have a semi-quantitative character only; more data will be taken in the future. The conclusion is warranted, though, that the sensitivity increases by turning on the jet. With the 1210-20W sensor, Θ_s = 30°C, and a jet speed of 3.3 cm/s, an increase in voltage output is observed of a factor 3 at frequencies from 100 to 300 Hz if the jet is directed vertically upward. When the jet is horizontal, no change in ac voltage output is seen. The speed of 3 cm/s is a factor 10 above the critical speed between free and forced convection, from Table 1. Apparently the free convection is still not negligible, since directing the jet vertically down results in a smaller improvement of the output over the no-jet situation.

3. DATA REDUCTION AND DISCUSSION OF RESULTS

3.1. Results for dc Heat Transfer

It is of interest to consider the relation of the Nusselt number Nu_{dc} to the relevant dimensionless number(s). Often the relation is given [23] in a form similar to Eq. (9):

$$Nu_{dc} = B(GrPr)^{m}. \tag{13}$$

Notice that the product GrPr is the Rayleigh number and may be considered as a Peclet number for free convection if Gr<<1.

A linear least-squares analysis was performed on the logarithmic version of Eq. (13)

$$\log Nu_{dc} = \log B + m\log(GrPr). \tag{14}$$

The results of this analysis for the three sensors show that the 1221-20 sensor does not fit in well with the other sensors. This can be understood by noticing that the 1211 sensor is arranged vertically and free convection from a vertical cylinder is different from that of a horizontal cylinder [26]. Without the 1211 data one finds for water B = 0.066 and m = 0.15 and for ethylene glycol B = 0.037 and m = 0.14.

3.2. Horizontal Particle Motion

The first point of concern is to check the expected quadratic dependence of the output voltage V_{ac} on the relative displacement ξ/d. The relative displacement at given frequency and temperature difference is proportional to the current through the shaker coil. This current was varied: 1, 2, and 3A. All through Tables 5, 6, and 7 the quadratic relation is quite well followed. There is some decrease at higher values of ξ/d, at about 2.5, which might indicate the appearance of the next higher term, a fourth power in ξ/d. The coefficient b in the relation between the rms Nusselt number Nu_{ac} and displacement

$$Nu_{ac} = b(\xi/d)^{2} \tag{15}$$

was found by averaging $V_{ac}/(\xi/d)^{2}$ for the three current values and multiplying the results by the ratio Nu_{ac}/V_{ac} (see Appendix A). This amounts to a least-squares adjustment whereby the observations are weighted inversely proportional to the square of their magnitude. If this weighting is not applied, the larger values of the observations overshadow the small ones. These values for

b are given in the next to last column in Tables 5, 6, and 7. It is most striking that in contrast to the results for vertical particle motion, this coefficient b is dependent on frequency. In some cases there is little variation with ω, see data sets 88-92, 93-97, 103-107, & 108-112. It also varies with sensor diameter but relatively little with temperature difference Θ_s. The dimensionless number next in line in the temperature Eq. (6) is the Fourier number $Fo = \kappa/\omega d^2$. The values of the inverse Fourier number are given in the last column to the right. There is an obvious correlation between the variation of b and the increase of Fo^{-1}. To study this quantitatively a least-squares regression was performed on a relation between b and the Fourier number of the form

$$\log b = \log c - m \log Fo. \tag{16}$$

The results are shown in Table 15 for each sensor at given Θ_s. From the least-squares regression one may derive an rms residual r according to the expression

$$r^2 = \frac{\sum (\log b_m - \log b_c)^2}{N - 2}, \tag{17}$$

where N is the number of observations in the regression, b_m is the measured value, and b_c is the calculated value. An "rms ratio" R_{rms} may be connected with r by $\log R_{rms} = r$. This ratio is used for comparison of the various regression models as a test on the goodness of fit. The results show that the exponent m is reasonably constant, but the coefficient c varies with the sensor diameter. Thus, the scaling with ω and d is not compatible with a $d^2\omega$ combination as implied by Fo or St scaling. If one pools the values for the same sensor at different Θ_s, one finds the following results. For a water medium: $c = 9.8\times10^{-3}$, $m = 0.55$, and $R_{rms} = 1.2$ for the 25-μm sensor; $c = 16.6\times10^{-3}$, $m = 0.69$, and $R_{rms} = 1.2$ for the 50-μm sensor; and $c = 64\times10^{-3}$, $m = 0.46$, and $R_{rms} = 1.4$ for the 150-μm sensor. In the case of glycol the corresponding numbers are: $c = 5.9\times10^{-3}$, $m = 0.31$, and $R_{rms} = 1.4$ for the 25-μm sensor; $c = 11.8\times10^{-3}$, $m = 0.34$, and $R_{rms} = 1.4$ for the 50-μm sensor; and $c = 7.4\times10^{-3}$, $m = 0.67$, and $R_{rms} = 1.6$ for the 150-μm sensor. All the

water data together give $c = 10.4\times10^{-3}$, $m = 0.90$, and $R_{rms} = 1.4$. All the glycol data together give $c = 4.5\times10^{-3}$, $m = 0.75$, and $R_{rms} = 1.6$.

The results for the coefficient c and exponent m for ethylene glycol differ considerably from those for water. This suggests that a factor other than the Fourier number is involved. Since the viscosity of ethylene glycol is much larger than that of water, one might assume that a combination of Pr and Gr would provide a better fit, in cooperation with the Fo regression. Therefore, a least-squares adjustment was performed on the expression

$$\log b = \log c + m_1 \log x_1 + m_2 \log x_2, \tag{18}$$

where the first variable x_1 may be chosen to be either Fo^{-1} or St^{-1}, while the second variable x_2 may be equated with Pr, Gr, or Ra(=GrPr). The involvement of Gr promises to rectify in part the scaling with respect to d and ω, which was poorly represented by the combination $d^2\omega$. Out of the six possible combinations a definite preference was shown for Fo and Gr, judging by the rms ratio, by the randomness of the measured value b_m divided by the computed value b_c, and by the standard deviations and cross correlations between the c, m_1, and m_2. Thus, the best fit appears to be given by the following expression for b:

$$b = 0.042\ Fo^{-0.56}\ Gr^{0.22}. \tag{19}$$

The results for all the values of b are given in Table 16. Of course, the product $0.042\ Gr^{0.22}$ is equivalent to the former (variable) coefficient c of the regression on Fo. This product is listed for comparison in the last column of Table 15.

The values and standard deviations are (1) $\log c = -1.38 \pm 0.03$, (2) $m_1 = 0.56 \pm 0.02$, (3) $m_2 = 0.22 \pm 0.01$ and the cross correlations are $\rho_{12} = -0.80$, $\rho_{13} = 0.83$, $\rho_{23} = -0.50$. The scaling in terms of d and ω implied by Eq. (19) is approximately $d^2\omega^{1/2}$.

The dependence of the coefficient b on the Fourier and Grashof numbers means that, given a constant ratio ξ/d, the sensor is more efficient for larger Grashof number and smaller Fourier number. Physically one might

Table 15 - Results of regression of b with respect to Fo and Fo,Gr

	Data	Sensor diam.	Θ_s	I: $b = c\ Fo^{-m}$, One sensor and Θ_s at a time — m	c 10^{-3}	R_{rms}	II: $b = c\ Fo^{-m_1}\ Gr^{+m_2}$, $c = 42.2\times10^{-3}$, $m_1 = 0.56$, $m_2 = 0.22$ — m_1	cGr^{m_2} 10^{-3}
Water	1-8	25	15°C	0 62	8.3	1.10	0.56	9.4
	9-16	50		0.72	13.4	1.15	0.56	15.2
	17-24	150		0.60	26.7	1.28	0.56	32.1
	25-32	25	30°C	0.52	9.6	1.13	0.56	12.2
	33-40	50		0.70	14.9	1.13	0.56	19.6
	41-48	150		0.41	7.7	1.12	0.56	41.6
	49-56	25	45°C	0.55	11.8	1.12	0.56	14.7
	57-64	50		0.66	22.3	1.14	0.56	23.7
	65-72	150		0.40	111	1.13	0.56	48.1
Ethylene Glycol	73-77	25	15°C	0.49	3.7	1.20	0.56	3.34
	78-82	50		0.62	4.7	1.41	0.56	5.35
	83-87	150		1.31	0.38	1.62	0.56	10.9
	88-92	25	30°C	0.189	6.93	1.25	0.56	4.45
	93-97	50		0.198	15.7	1.09	0.56	7.02
	98-102	150		0.348	28.3	1.32	0.56	14.7
	103-107	25	45°C	0.254	8.2	1.17	0.56	5.51
	108-112	50		0.206	22.2	1.11	0.56	8.78
	113-117	150		0.36	37.2	1.24	0.56	18.2

tentatively interpret this as follows. The inverse Fourier number expresses the ratio of local heating to heat transport by conduction. If this ratio is small, the acoustically induced heating and cooling are obviously small compared with the average heat conduction. The dependence on the Grashof number suggests that for small values of Gr the hot film is surrounded by a viscosity dominated region extending many diameters from the sensor, on which the variable acoustic flow has little influence. For larger Gr the viscous region is reduced to a boundary-type layer, and the cooling effect of the acoustic flow can approach the hot film more closely.

The pattern of phase variation with frequency (Fig. 3) also changes with d and ω; a complete study of its scaling properties has yet to be done. It is possible that a simpler scaling law could be discovered for in-phase and out-of-phase components separately (with respect to the phase of the pressure or displacement in the main body of the medium). Of course, this could not be used for measurement of an unknown field since the absolute phase would not be known, but it might be useful for better insight into the heat transfer process.

Table 16 - Calculated value b_c and ratio of measured to calculated value.

b_m/b_c for regression log b = log c - $m_1$logFo + $m_2$logGr

logc = -1.38 ±0.03; m_1 = 0.56 ±0.02; m_2 = 0.22 ±0.01

#	b_c 10^{-3}	b_m/b_c	#	b_c 10^{-3}	b_m/b_c	#	b_c 10^{-3}	b_m/b_c	#	b_c 10^{-3}	b_m/b_c
1	6.42	0.93	33	29.2	0.96	65	247	1.58	93	13.4	1.55
2	7.12	0.87	34	32.3	0.90	66	274	1.41	94	19.8	1.03
3	9.47	0.91	35	43.1	0.93	67	365	1.27	95	27.2	1.02
4	10.5	0.77	36	47.8	0.76	68	404	0.96	96	33.2	0.85
5	13.2	1.02	37	60.0	1.10	69	508	1.30	97	40.1	0.71
6	14.0	0.96	38	63.6	1.04	70	538	1.22	98	98.3	1.03
7	17.6	0.90	39	80.0	1.07	71	677	1.02	99	145	0.79
8	20.7	1.03	40	93.8	1.27	72	794	1.08	100	199	0.69
9	22.8	1.15	41	216	1.34				101	244	0.47
10	25.3	1.06	42	239	1.18				102	293	0.86
11	33.6	1.14	43	319	1.09				103	4.82	1.50
12	37.3	0.88	44	353	0.86				104	7.12	1.33
13	46.8	1.25	45	443	1.07	73	2.90	1.26	105	9.73	1.37
14	49.7	1.22	46	470	0.94	74	4.28	1.07	106	11.9	1.00
15	62.5	1.27	47	591	0.88	75	5.85	1.05	107	14.4	0.77
16	73.3	1.62	48	695	0.99	76	7.15	0.83	108	16.8	1.64
17	168	1.16	49	9.90	0.80	77	8.64	1.26	109	24.9	1.27
18	186	1.03	50	11.0	0.78	78	10.2	1.25	110	34.0	1.27
19	248	0.93	51	14.6	0.85	79	15.0	0.88	111	41.7	0.95
20	275	0.74	52	16.2	0.73	80	20.5	0.73	112	50.3	0.78
21	345	0.85	53	20.3	0.94	81	25.2	1.00	113	122	1.16
22	366	0.75	54	21.6	0.89	82	30.4	1.57	114	180	0.85
23	460	0.97	55	27.1	0.82	83	72.1	0.68	115	247	0.69
24	541	1.48	56	31.9	0.68	84	107	0.55	116	301	0.61
25	8.30	0.80	57	34.9	1.11	85	146	0.69	117	364	0.90
26	9.18	0.79	58	38.7	1.06	86	178	1.73			
27	12.2	0.82	59	51.6	1.17	87	215	2.84			
28	13.6	0.71	60	57.2	0.86	88	3.87	1.63			
29	17.0	0.93	61	71.8	1.19	89	5.72	1.25			
30	18.1	0.86	62	76.2	1.07	90	7.82	1.33			
31	22.7	0.78	63	95.6	1.18	91	9.56	1.14			
32	26.7	0.64	64	113	1.41	92	11.6	0.65			

3.3. Vertical Particle Motion

Inspection of Tables 13 and 14 shows that Nu_{ac} is quite well represented by a linear relationship with respect to the relative displacement, since it varies proportionally to the current through the calibrator coil. The coefficient a in the relation

$$Nu_{ac} = a(\zeta/d) \tag{20}$$

was computed by averaging $Nu_{ac}/(\zeta/d)$ for the various current values. This amounts to a least-squares regression whereby the observed values are weighted by a factor inversely proportional to the magnitude squared of the measurement.

It is seen that the value of a is reasonably independent of frequency within the accuracy limits of the experiment. Since the ac particle motion is superimposed on the free convection, it is logical to attempt a regression of the coefficient a on the Grashof or Rayleigh number. Figure 6 shows the relationship for the two sets of data in 1982 and 1983. It is quite striking that the data appear to fall on two distinct lines not related to sensor type or time of measurement. No explanation for this unfortunate discrepancy has been found to date. It is possible that the formation of bubbles, as described in Section 2.2, played a role; but it is difficult to see how this would have created two distinct lines and not a continuum of values. A least-squares regression was performed on the data of the two separate cases with the logarithmic dependence

$$\log a = \log c_{Ra} + m_{Ra} \log Ra. \tag{21}$$

The fit for the two sets was quite good. The values for the coefficient c_{RA} and the exponent m_{Ra} were 0.217 and 0.360 with $R_{rms} = 1.04$ for the upper line and 0.130 and 0.315 with $R_{rms} = 1.06$ for the lower line. The data coverage was insufficient to distinguish between Gr and Ra as the better independent variable. To resolve this question, measurements with ethylene glycol in the calibrator would be in order.

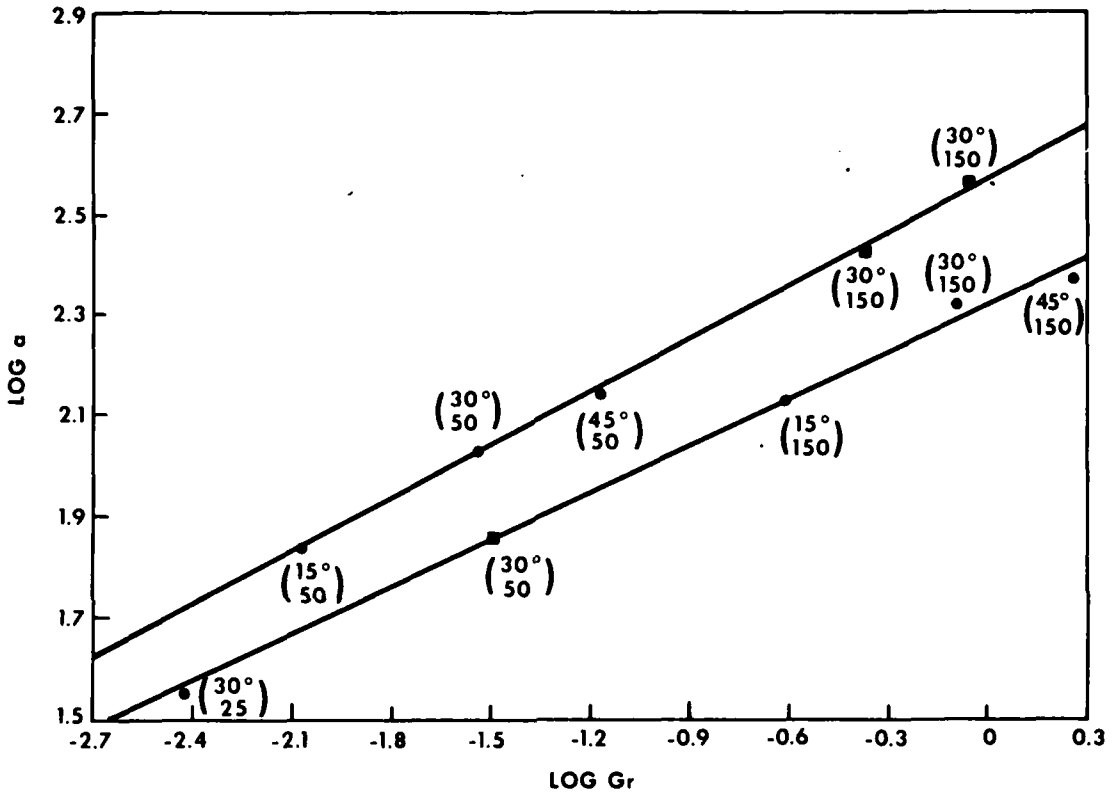

The upper number between parentheses is the temperature difference Θ_s.
The lower number is the sensor diameter in μ.
● - data of Jul 83
■ - data of Jul-Aug 82.

Fig. 6 - Coefficient of relation $Nu_{ac} = a(\zeta/d)$ as a function of Grashof number.

4. CONCLUSIONS AND SUGGESTIONS FOR FURTHER WORK

The present study shows that hot-film anemometry can be successfully applied to the detection of particle motion in hydroacoustic fields. Its sensitivity at constant intensity increases for decreasing frequency, in contrast to velocity hydrophones based on accelerometers. It is felt that, conversely, the anemometer response to harmonic acoustic fields may also be used as a tool to study free convection about a cylinder.

The prime area to be developed is the detection of particle motion under imposed bias flow. It has greater sensitivity, frees the experiment of the dependence on the direction of gravity, and adds a valuable control on determination of direction of the acoustic motion.

The discrepancy in the data in vertical particle motion should be investigated.

Further investigation of the empirical relations in terms of dimensionless groups is in order, including also the variation in phase.

Overall improvement of the accuracy of the measurements, which at this time is estimated at about 10 to 20%, appears useful. This would include modifications of trough and vertical calibrator.

5. ACKNOWLEDGMENTS

The suggestion by Dr. Anthony J. Rudgers of this laboratory to attempt acoustic detection by hot-film anemometry and his discerning discussions in the initial stages of the project are gratefully acknowledged. The dedication and care devoted by Ms. Susan E. Eveland to data collection and reduction are greatly appreciated.

REFERENCES

1. C. B. Leslie, J. M. Kendall, and J. L. Jones, "Hydrophone for measuring particle velocity," J. Acoust. Soc. Am. 28, 711-715, 1956.

2. T. A. Henriquez, "A standard pressure gradient hydrophone," J. Acoust. Soc. Am. Suppl. 1, 70, S100, 1981.

3. P. S. Dubbelday, "Measurement of particle velocity in a hydroacoustic field by hot-film anemometry," J. Acoust. Soc. Am. Suppl. 1, 70, S102 and S103, 1981.

4. R. F. Blackwelder, "Hot-wire and hot-film anemometry," in "Methods of Experimental Physics, Vol. 18, Fluid Dynamics," Editor R. Y. Emerich (Academic Press, New York, 1981) p. 269.

5. P. Bradshaw, "The hot-wire anemometer," Chapter 5 of An Introduction To Turbulence And Its Measurement (Pergamon Press, Oxford, 1971).

6. G. Comte-Bellot, "Hot-wire anemometry," Annual Review of Fluid Mechanics, Vol. 8, 1972, pp 209-231.

7. M. R. Davis, "Hot-wire anemometer response in a flow with acoustic disturbances," J. Sound & Vibr. 56, 565-570, 1978.

8. F. K. Deaver, W. R. Penney, and T. B. Jefferson, "Heat transfer from an oscillating horizontal wire to water," Trans. of ASME J. Heat Transf. 84, 251-256, 1962.

9. W. R. Penney and T. B. Jefferson, "Heat transfer from an oscillating horizontal wire to water and ethylene glycol," Trans. of ASME J. Heat Transf. 88, 359-366, 1966.

10. R. M. Fand and J. Kaye, "The influence of sound on free convection from a horizontal cylinder," Trans. of ASME J. Heat Transf. 83, 133-148, 1961.

11. R. M. Fand, "The influence of acoustic vibration on heat transfer by natural convection from a horizontal cylinder to water," Trans. of ASME J. Heat Transf. 87, 309-310, 1965.

12. R. Lemlich and M. A. Rao, "The effect of transverse vibration on free convection from a horizontal cylinder," Int. J. Heat & Mass Transf. 8, 27-33, 1965.

13. L. V. King, "On the convection of heat from small cylinders in a stream of fluid. Determination of convection constants of small platinum wires with application to hot-wire anemometry," Phil. Trans. A 214, 381 (1914).

14. D. J. Tritton, Physical Fluid Dynamics (Van Nostrand Reinhold Co., New York, 1977), pp. 155-161.

15. R. S. Tomasello, "The Boussinesq Approximation," Master's Thesis, Florida Institute of Technology, 1973.

16. A. J. Ede, "Advances in free convection," in Advances in Heat Transfer Vol. 4, Ed. J. P. Hartnett and T. F. Irvine, (Academic Press, New York, 1967).

17. V. T. Morgan, "The overall convective heat transfer from smooth circular cylinders," in Advances in Heat Transfer Vol. 11, Ed. T. F. Irvine and J. P. Hartnett (Academic Press, New York, 1975).

18. Y. Jaluria, Natural Convection, Heat and Mass Transfer (Pergamon Press, Oxford, 1980).

19. H. Lamb, Hydrodynamics (Dover Publications, New York, 1945).

20. G. K. Batchelor, Introduction to Fluid Dynamics (Cambridge U. Press, Cambridge, 1967) pp. 240-246.

21. Ref. 17, p. 216.

22. Ref. 4, p. 271.

23. Ref. 17, p. 201.

24. Ref. 18, p. 87.

25. Anon., "Underwater Electroacoustic Standard Transducers Catalogue," Naval Research Laboratory, Underwater Sound Research Detachment, May 1982.

26. Ref. 18, pp. 86 & 96.

Appendix A

COMPUTATION OF DIMENSIONLESS NUMBERS

Most of the data on the properties of glycol and water were taken from Ref. A1. The data for the expansion coefficient of ethylene glycol are found in Ref. A2. The data near 40°C were interpolated by a second-degree polynomial through the data points at 20, 40, and 60°C. T is in degree Celsius.

For water:

$$k(W\ m^{-1}K^{-1}) = 0.552 + 2.35\times10^{-3}T - 11.2\times10^{-6}T^2$$

$$\nu(m^2s^{-1}) = 1.522\times10^{-6} - 30.0\times10^{-9}T + 0.210\times10^{-9}T^2$$

$$\alpha(K^{-1}) = -12.87\times10^{-6} + 11.99\times10^{-6}T - 0.0509\times10^{-6}T^2$$

$$Pr = 11.06 - 0.236T + 1.7\times10^{-3}T^2.$$

For ethylene glycol:

$$k(Wm^{-1}K^{-1}) = 0.239 + 0.575\times10^{-3}T - 3.75\times10^{-6}T^2$$

$$\nu(m^2s^{-1}) = 36.23\times10^{-6} - 1.016\times10^{-6}T + 8.19\times10^{-9}T^2$$

$$\alpha(K^{-1}) = 0.556\times10^{-3} + 8.70\times10^{-6}T - 0.145\times10^{-6}T^2$$

$$Pr = 384 - 10.7T + 86.3\times10^{-3}T^2.$$

The material parameters are computed at an average temperature of the sensor and medium temperatures $(T_s + T_o)/2$. The Nusselt number is defined as $Hd/k\Theta_s$, where H is the heat flux. H is computed from the measured bridge voltage in the following way. The sensor resistance R is in series with the bridge resistor R_b in the anemometer bridge, with a value $R_b = 40\ \Omega$. The resistance measured in the bridge R_t includes the resistance of the cable, probe-holder, and probe in addition to the sensor resistance itself. The cable resistance is 0.1 Ω, that of the probe-holder is 0.08 Ω, and the resistance R_p of the probe varies with the given sensor.

The heat transfer rate $\dot{Q}$ is given by

$$\dot{Q} = \frac{V_{dc}^2 R}{(R_t+R_b)^2}. \qquad \text{(A1)}$$

For a typical measurement with a 1210-20W sensor with $\Theta_s = 30^0$, $R = 6\ \Omega$, one finds $V_{dc} = 4.78$ V. Thus $\dot{Q} = 64$ mW. The heat flux is determined by

$$H = \dot{Q}/\pi \ell d \tag{A2}$$

and the dc Nusselt number Nu_{dc} by

$$Nu_{dc} = V_{dc}^2 R/\pi \ell k \Theta_s (R_t + R_b)^2. \tag{A3}$$

The factor needed to convert amplitude or rms value of the ac voltage to the corresponding value for the Nusselt number variation is given by $Nu_{ac}/V_{ac} = 2Nu_{dc}/V_{dc}$.

REFERENCES

A1. E. R. G. Eckert and R. M. Drake, Jr., Analysis of Heat and Mass Transfer, (McGraw Hill, New York, 1972) pp. 777 and 779.

A2. "Handbook of Chemistry and Physics," R. C. Weast Ed., 53rd Edition, The Chemical Rubber Co., 1972, p. F5.

Appendix B

TROUGH AND SHAKER ARRANGEMENT

The horizontal particle movement is produced by a trough, especially designed for this application, attached to a horizontal shaker (Fig. B1). The original trough was made of a polyvinyl chloride (PVC) cylinder with 6.35-mm (1/4-in.) wall thickness and 12.7-mm (1/2-in.)-thick lucite endplates. The PVC trough was suspended by 1.5-m (60-in.) cables from the ceiling. An improved version was constructed of steel. Its dimensions are shown in cross section in Fig. B2. Notice that the trough has a free surface of the liquid. A similar device was described by Bauer [B1], based on a closed cylinder. A later version has a free surface [B2]. The steel trough was suspended from an A-frame with four steel wires of 0.76-mm (0.030-in.) diam. and 20-cm length.

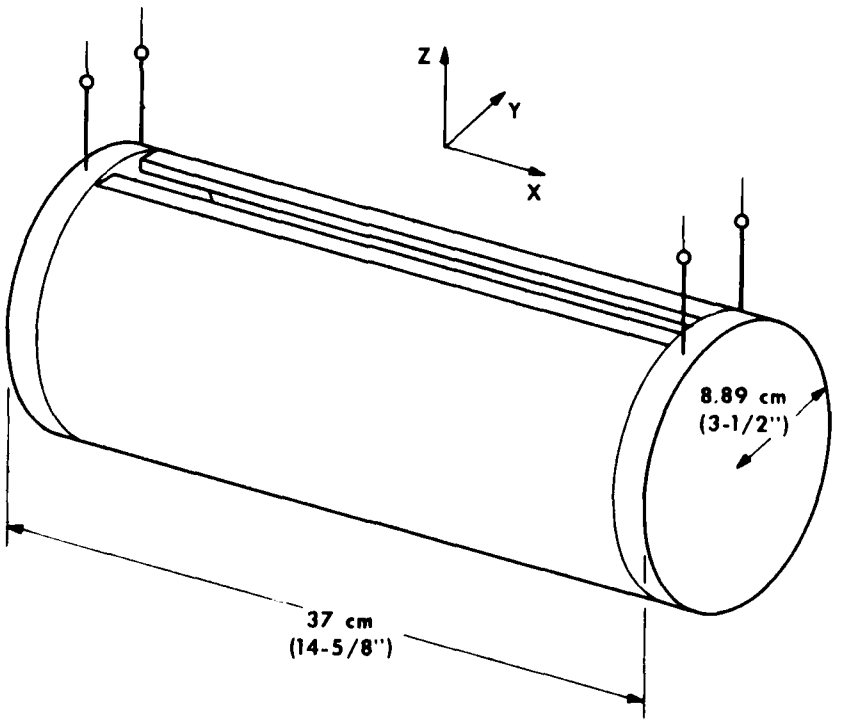

Fig. B1 - Trough for horizontal particle motion

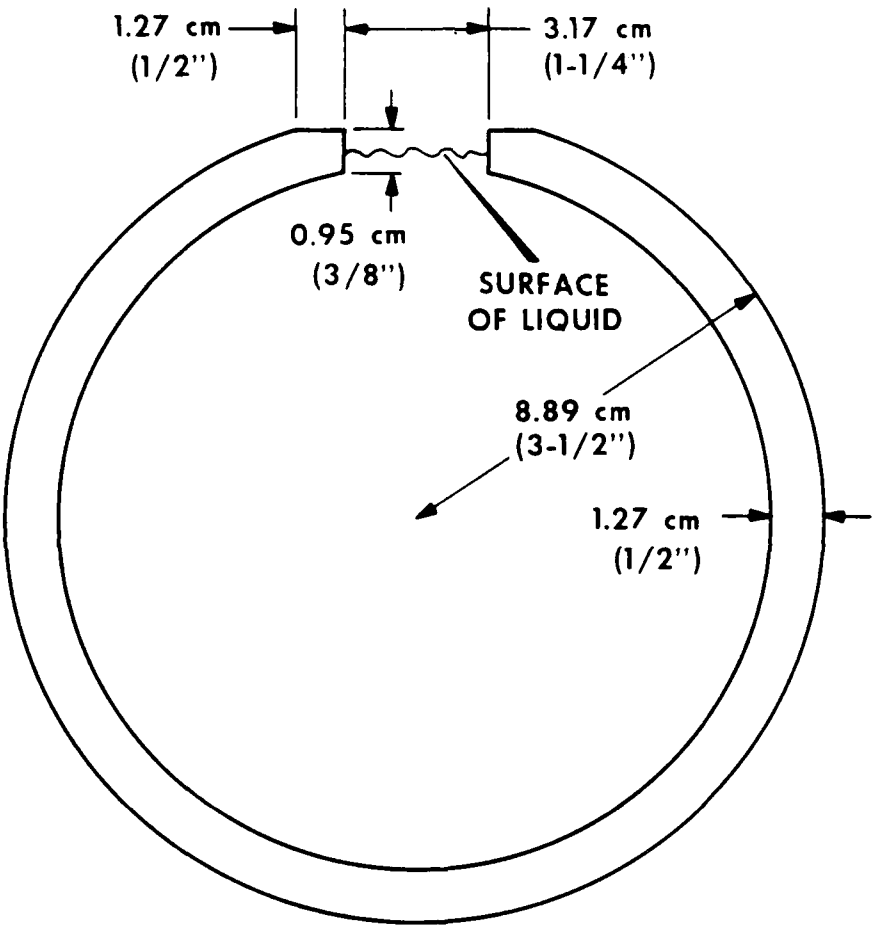

Fig. B2 - Cross section of steel trough

Analysis of the resulting motion is more complicated as a consequence of the free surface, especially for a cylindrical geometry. One may readily solve the equation of motion under the proper boundary conditions for a rectangular trough. Although the frequencies are rather low in the present study, it is assumed for generality that the pressure is a solution of Helmholtz's equation

$$(\nabla^2 + k_o^2)p = 0, \tag{B1}$$

where k_o is the wavenumber in the medium $k_o = \omega/c_o$, with c_o the propagation speed. As to the boundary conditions, assuming rigidity of the trough, the end faces at $x = \pm L/2$ impose a condition on the velocity

$$u(-L/2,z) = u(L/2,z) = U \tag{B2}$$

and the vertical velocity w is zero at the bottom and thus the pressure gradient

$$\frac{\partial p}{\partial z} = 0 \text{ at } z = 0. \tag{B3}$$

It is assumed that the surface variations are not important dynamically, thus diverging from the usual development of surface waves, to give

$$p(x,h) = 0, \tag{B4}$$

where h is the water depth. The solution for pressure and velocity components is

$$p = \frac{-4i\rho\omega U}{\pi} \sum_0^\infty \frac{(-1)^n}{k_n(2n+1)} \frac{\sinh k_n x}{\cosh k_n L/2} \cos\left[\frac{(2n+1)\pi}{2}\frac{z}{h}\right] \tag{B5}$$

$$u = \frac{4}{\pi} U \sum_0^\infty \frac{(-1)^n}{(2n+1)} \frac{\cosh k_n x}{\cosh k_n L/2} \cos\left[(2n+1)\frac{\pi z}{2h}\right] \tag{B6}$$

$$w = \frac{-2U}{h} \sum_0^\infty \frac{(-1)^n}{k_n} \frac{\sinh k_n x}{\cosh k_n L/2} \sin\left[(2n+1)\frac{\pi z}{2h}\right] \tag{B7}$$

where $k_n^2 = (2n+1)^2(\frac{\pi}{2h})^2 - k_o^2$. For low frequencies such that $h<<\lambda$ one may ignore k_o. The leading term in the x dependence of the pressure is $\sinh \frac{\pi x}{2h}$ and this S-shape is recognized in the following picture (Fig. B3).

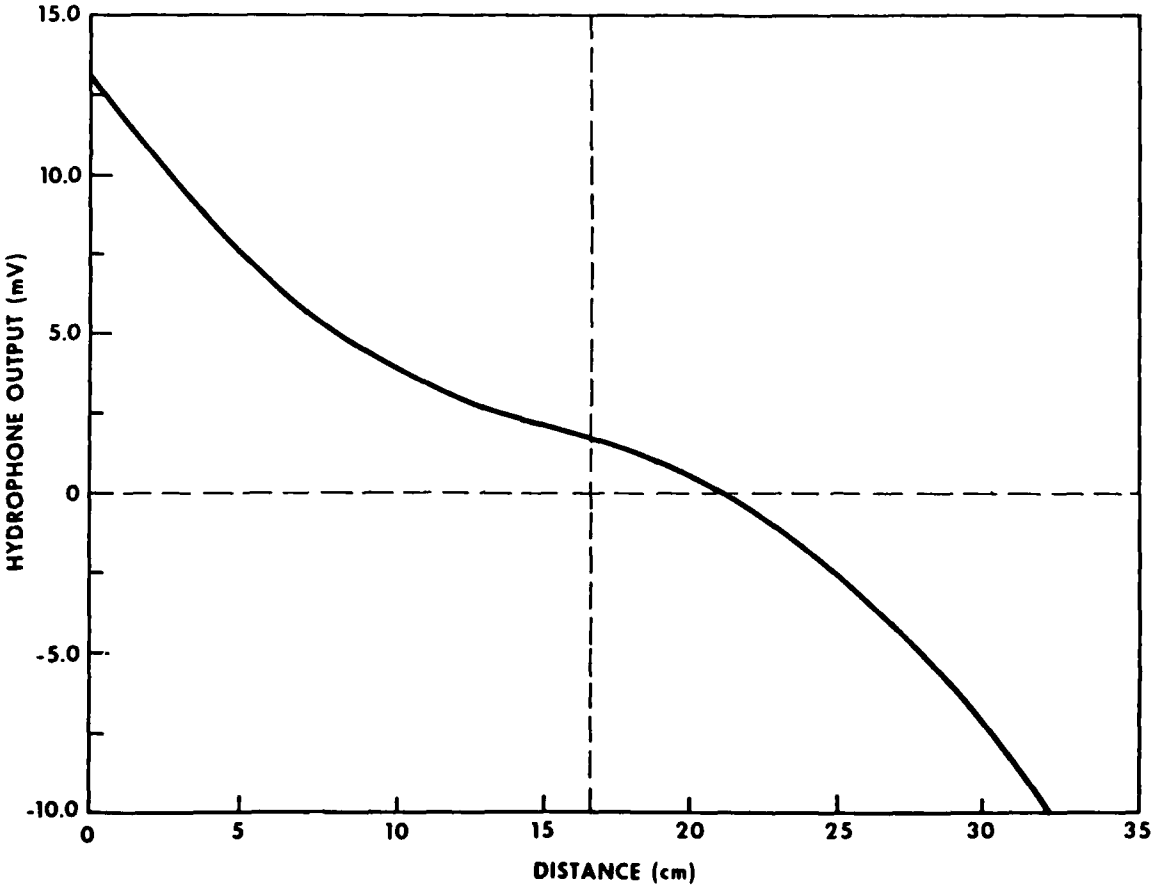

Fig. B3 - Output from F61 standard hydrophone as a function of location along the axis of PVC trough.
The solid curve is a fourth-degree polynomial fit.

The trough is connected to a horizontal shaker. The pressure is measured by a USRD type F61 standard hydrophone [B3]. Figure B3 shows the pressure variation along the axis of the PVC trough starting from the side attached to the shaker. The solid curve is a fourth-degree polynomial fit.

Figure B4 gives the pressure profile for the steel trough. The symmetry of the curve about the center of the trough has obviously improved thanks to the greater rigidity of the steel. Moreover, the slit in the top of the cylinder was smaller than for the PVC trough. Thus the free surface was smaller than in that case. As a consequence the vertical pressure gradient needed to accelerate fluid towards the free surface is less. Therefore the S is less deep and more like the straight line that would prevail for a completely closed cylinder. The polynomial fit served to find the derivative in the center of the trough where the hot-film anemometer measurements were performed. A set of derivative curves at various frequencies is shown in Fig. B5 in terms of the relative displacement (ξ/d).

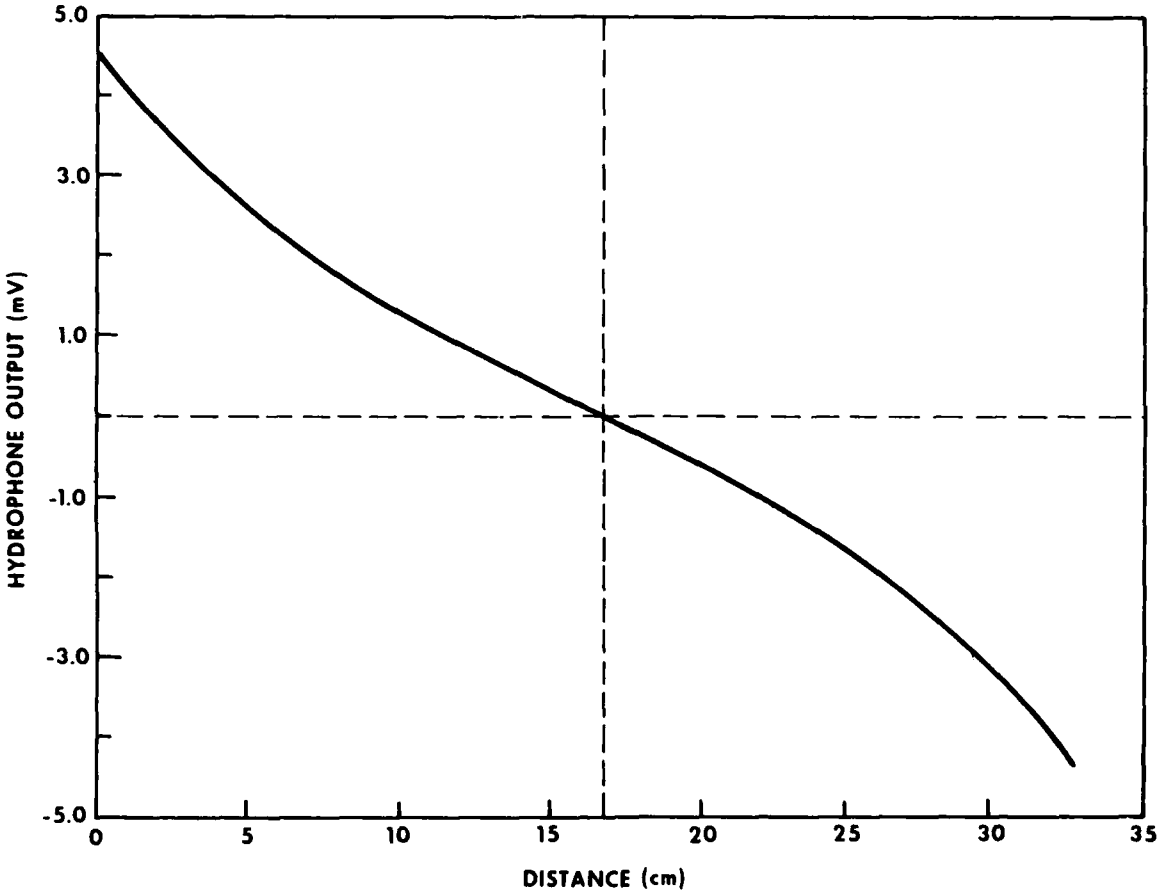

Fig. B4 - Response of F61 standard transducer to pressure field in water-filled steel trough. 1 mV corresponds to 19 Pa. Solid curve is a cubic least-squares fit.

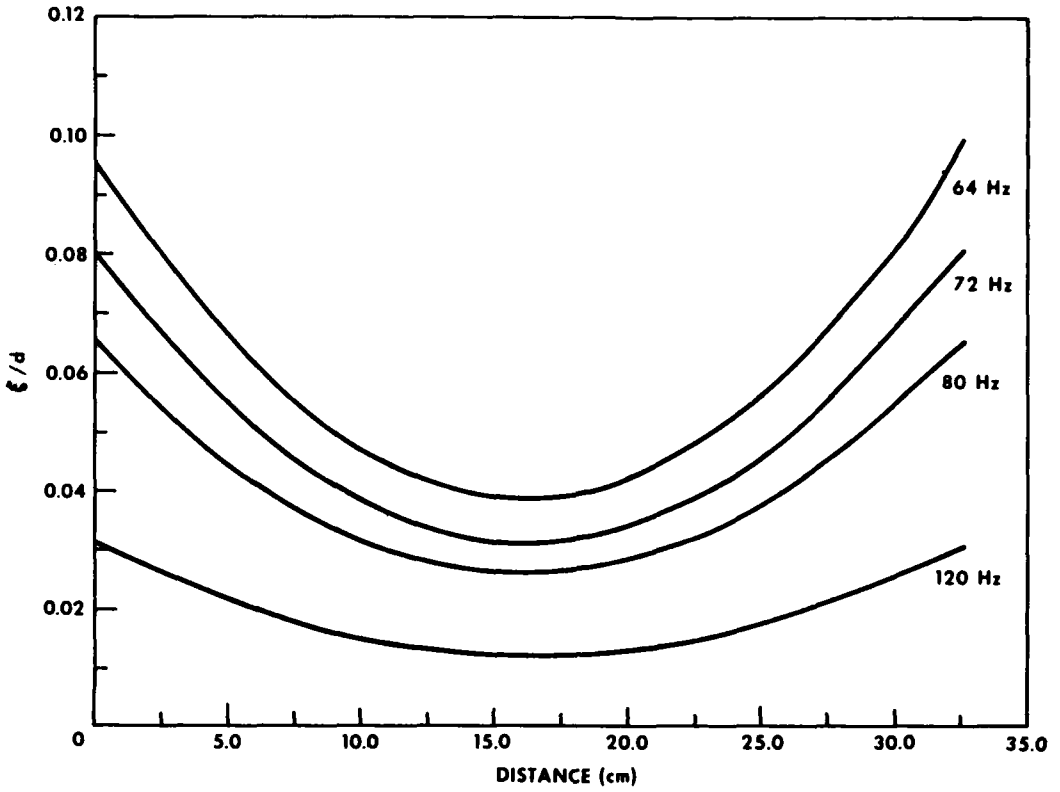

Fig. B5 - Relative displacement in steel trough as a function of distance along axis for various frequencies; d = 50μ

REFERENCES

B1. B. B. Bauer, "Laboratory calibrator for gradient hydrophones," J. Acoust. Soc. Am. 39, 585-586, 1966.

B2. B. B. Bauer, L.A. Abbagnero, and J. Schumann, "Wide-range calibration system for pressure-gradient hydrophones," J. Acoust. Soc. Am. 51, 1717-1724, 1972.

B3. Anon., "Underwater Electroacoustic Standard Transducers Catalogue," Naval Research Lab., Underwater Sound Reference Detachment, May 1982, p. 71.

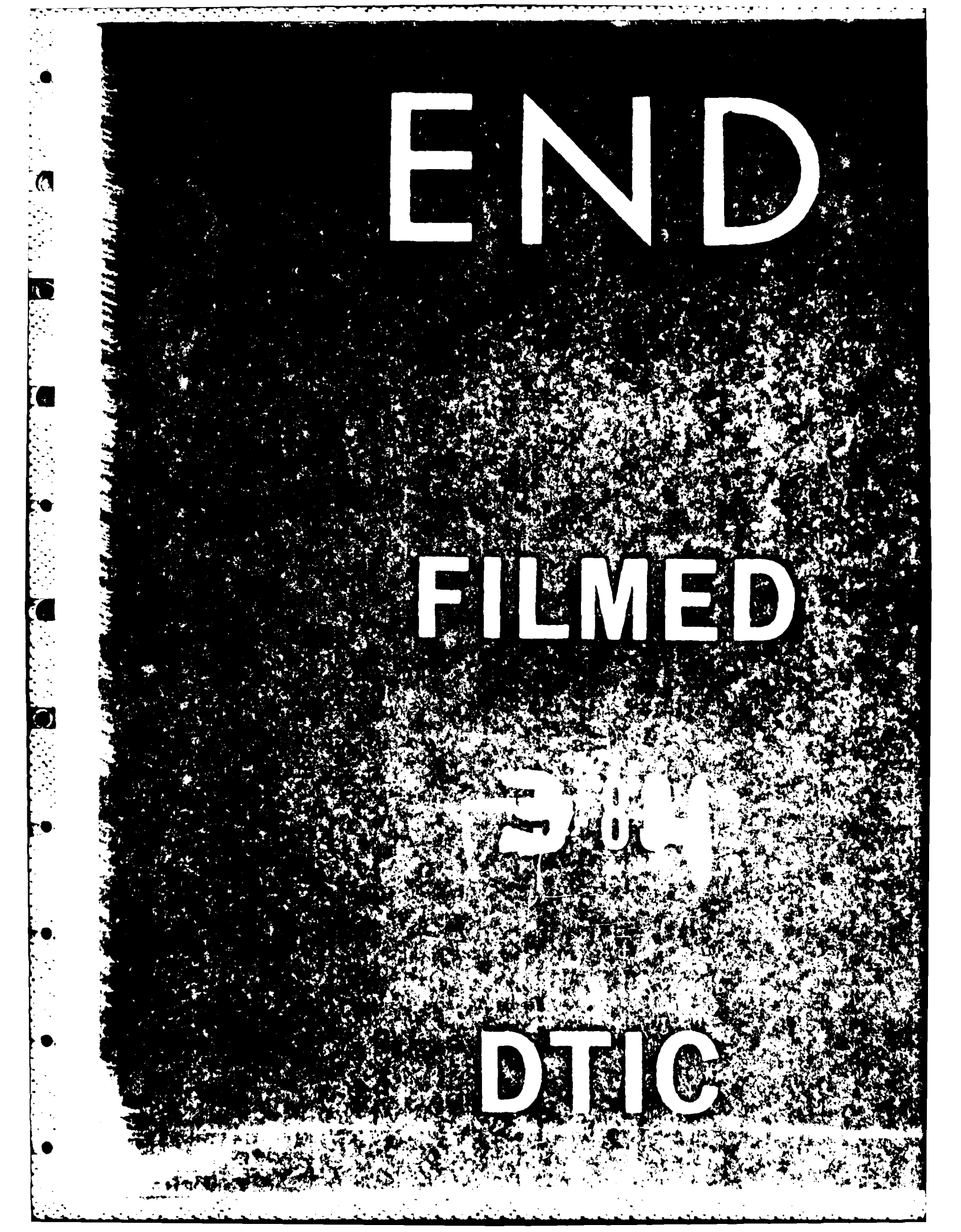
END
FILMED
DTIC